ADDIS ABABA UNIVERSITY

SCHOOL OF GRADUATE STUDIES

ADDIS ABABA INSTITUTE OF TECHNOLOGY (AAiT)

ELECTRICAL AND COMPUTER ENGINEERING DEPARTMENT

Performance Evaluation of Receivers for Ultra-Wideband Wireless Communication Systems

By

Welelaw Yenieneh Lakew

Advisor

Dr. Eneyew Adugna

A Thesis Submitted to the School of Graduate Studies of Addis Ababa University in Partial Fulfillment of the Requirements for the Degree of

Masters of Science

In

Electrical Engineering

July, 2011

Addis Ababa, Ethiopia

ADDIS ABABA UNIVERSITY
SCHOOL OF GRADUATE STUDIES
ADDIS ABABA INSTITUTE OF TECHNOLOGY (AAiT)
ELECTRICAL AND COMPUTER ENGINEERING DEPARTMENT

Performance Evaluation of Receivers for Ultra-Wideband Wireless Communication Systems

By

Welelaw Yenieneh Lakew

Approval by Board of Examiners

Dr.-Ing. Getahun Mekuria	_____
Chairman, Dept. Graduate Committee	Signature
Dr. Eneyew Adugna	_____
Advisor	Signature
Dr.-Ing. Getahun Mekuria	_____
Internal Examiner	Signature
Dr.-Ing. Hailu Ayele	_____
External Examiner	Signature

Declaration

I, the undersigned, declare that this thesis is my original work, has not been presented for a degree in this or any other university, and all sources of materials used for the thesis have been fully acknowledged.

Welelaw Yenieneh Lakew _____

Name Signature

Place: **Addis Ababa**

Date of Submission: **August 12, 2011**

This thesis has been submitted for examination with my approval as a university advisor.

Dr. Eneyew Adugna _____

Advisor's Name Signature

Abstract

Ultra Wide Band (UWB) is a promising technology for short range broadband wireless data communication, sensor networks, radar imaging and target identification, location finding and positioning applications. This technology is the best choice for short range wireless communication systems since it is cost-effective, power-efficient and has extremely higher data rates. Any wireless system that has a fractional bandwidth greater than or equal to 20% or a total bandwidth larger than or equal to 500MHz enters in the UWB definition. The Federal Communications Commission (FCC) has allocated 7.5GHz of spectrum for unlicensed use of ultra-wideband (UWB) devices in the 3.1 to 10.6 GHz frequency band and limits the maximum power spectral density (PSD) of the transmitted signal to -41.3dBm/MHz.

The main subject of this thesis is to evaluate bit error rate (BER) performance of RAKE and adaptive MMSE receivers for UWB wireless communication systems. First, bit error rate (BER) performance of RAKE receiver on standard IEEE 802.15.3a channel model has been simulated. Here, the BER performance of RAKE receiver for different RAKE types, number of RAKE fingers, combining techniques, length of bit repetition codes, transmitted signal formats and channel types has been evaluated and compared for single user scenario. The simulation results show that an ideal ARAKE receiver using TH-BPSK-UWB transmitted signal format, MRC technique and applying bit repetition coder has the best performance. Then, bit error rate (BER) performance of adaptive MMSE receiver using LMS, NLMS and RLS adaptive algorithms has been evaluated and analyzed on standard IEEE 802.15.3a channel model for different number of users and the simulation results illustrate that adaptive MMSE receiver using RLS algorithm has the best BER performance. Finally, BER performance SRAKE receiver with 5 and 10 fingers has been compared with BER performance adaptive MMSE receiver using the above three adaptive algorithms for single user scenario. The simulation result describes that adaptive MMSE receiver using all the above three algorithms has by far the best BER performance compared to SRAKE receiver with 5 and 10 fingers. All the above simulations have been conducted using MATLAB software.

Key Words: UWB, RAKE Receiver, Adaptive MMSE Receiver, LMS, NLMS, RLS, Modulation, Multiple Access, Spread Spectrum, WPAN

Acknowledgements

This thesis work has been accomplished successfully with the support and encouragement of numerous individuals who deserve heartfelt acknowledgment.

First and foremost, I would like to express my sincere gratitude to my advisor, Dr. Eneyew Adugna, for giving me the opportunity to do my thesis in this interesting and challenging field. I am thankful to him for providing me guidance, encouragement and constructive feedback in my research throughout the year. His advice and help were absolutely invaluable for the successful completion of my thesis work.

I am also very grateful to all of my colleagues for their moral and material support during my thesis work. Particularly, I am greatly indebted to Ato Demissu Taye, Ato Melaku Yigzaw and Ato Workineh Abiyu for their unlimited support to complete my thesis in time.

Last but not least, I would like to express my deepest gratitude to my parents, brothers and sisters. Without their love, support and encouragement, it would be impossible for me to achieve what I have done.

Above all, I praise Lord who has given me the strength and patience to achieve my goals, who has surrounded me with the greatest family, friends and colleagues and who is always with me both in time of difficulty and happiness. One thing that always comes into my mind in time of challenge is "……for with God all things are possible" (Mark 10:27).

Table of Contents

List of Figures

List of Tables

List of Acronyms

AWGN	Additive White Gaussian Noise
BER	Bit Error Rate
BPSK	Binary Phase Shift Keying
CDMA	Code division multiple access
CMF	Classical Matched Filter
DCS	Digital communication system
DS	Direct Sequence
ECG	Equal Gain Combining
EIRP	Effective isotropic radiated power
FCC	Federal Communications Commission
FIR	Finite Impulse Response
GPS	Global Positioning Systems
GSM	Global system for mobiles
IEEE	Institute of Electrical and Electronic Engineering
ISI	Inter Symbol Interference
ISM	Industrial, Scientific and Medical
IR	Impulse Radio
LMS	Least Mean Square
LOS	Line of Sight
MAI	Multiple Access Interference

MMSE	Minimum Mean Square Error
MRC	Maximum Ratio Combining
NBI	Narrow Band Interference
NLMS	Normalized Least Mean Square
NLOS	Non Line of Sight
OFDM	Orthogonal Frequency Division Multiplexing
OOK	On-Off Keying
PAM	Pulse Amplitude Modulation
PPM	Pulse Position Modulation
PSD	Power Spectral Density
RLS	Recursive Least Square Error
SC	Selective Combining
SNR	Signal to Noise Ratio
TH	Time Hopping
UMTS	Universal mobile telecommunications system
UNII	Unlicensed national information infrastructure
UWB	Ultra Wide Band
WBAN	Wireless Body Area Network
Wi-Fi	Wireless Fidelity
WPAN	Wireless Personal Area Network
WLAN	Wireless Local Area Network

Chapter 1
Introduction

1.1. Overview of UWB wireless Communication Systems

Ultra-wideband (UWB) has emerged as a technology that offers great promise to satisfy the growing demand for low-cost, high-speed digital wireless indoor and home networks. The enormous bandwidth available, the potential for high data rates, and the potential for small size and low processing power along with low implementation cost all present a unique opportunity for UWB to become a widely adopted radio solution for future wireless home-networking technology. Currently, UWB technology is able to support various data rates, ranging from 100 to 500 Mbps within a distance of 20 meters.

1.1.1. Definition of UWB

Ultra wideband (UWB) is a technology that uses short-duration (picoseconds to nanoseconds) pulses for transmission and reception of information. Since frequency is inversely related to time, the short-duration UWB pulses spread their energy across a wide range of frequencies from near DC to several gigahertzes (GHz) with very low power spectral density (PSD). The average transmission power of a UWB system is very low (usually in the order of microwatts) due to low duty cycle short-duration UWB pulses.

According to FCC's definition, any signal with a bandwidth wider than 500 MHz or a fractional bandwidth greater than 20% can be considered as UWB. The fractional bandwidth is defined as the ratio of signal bandwidth to the center frequency [19] and is given by:

$$B_f = \frac{BW}{f_c} = \frac{(f_H - f_L)}{(f_H + f_L)/2} \tag{1.1}$$

Where f_H and f_L are the highest and the lowest transmitted frequencies at –10 dB emission point, respectively, BW is the signal bandwidth and f_c is the center frequency.

1.1.2. FCC Mask

The bandwidth of UWB signals requires a strict regulation of their transmission spectrum in order to avoid interference with other coexisting narrowband and wideband wireless communication systems. Indeed, many systems, whether licensed or not, are presented in UHF

and SHF bands, which are very favorable for radio systems deployment. To allow the use of UWB signals over several GHz, regulatory authorities imposed a strict limitation on the transmission power. Figure 1.1 shows some radio systems existing in UHF and SHF bands. We can note that there are reserved bands for several systems like the standards of cellular telephony GSM (900 MHz), DCS (1.8 GHz) and UMTS (2 GHz). The global positioning system (GPS) also occupies a reserved band around 1.5 GHz. Other frequency bands are already used for unlicensed communication systems. For example, the ISM band is used by systems such as Bluetooth, WiFi and DECT, and is also authorized for domestic devices such as microwave ovens. The UNII band is the frequency band where the WiFi 802.11a and HiperLAN standards operate.

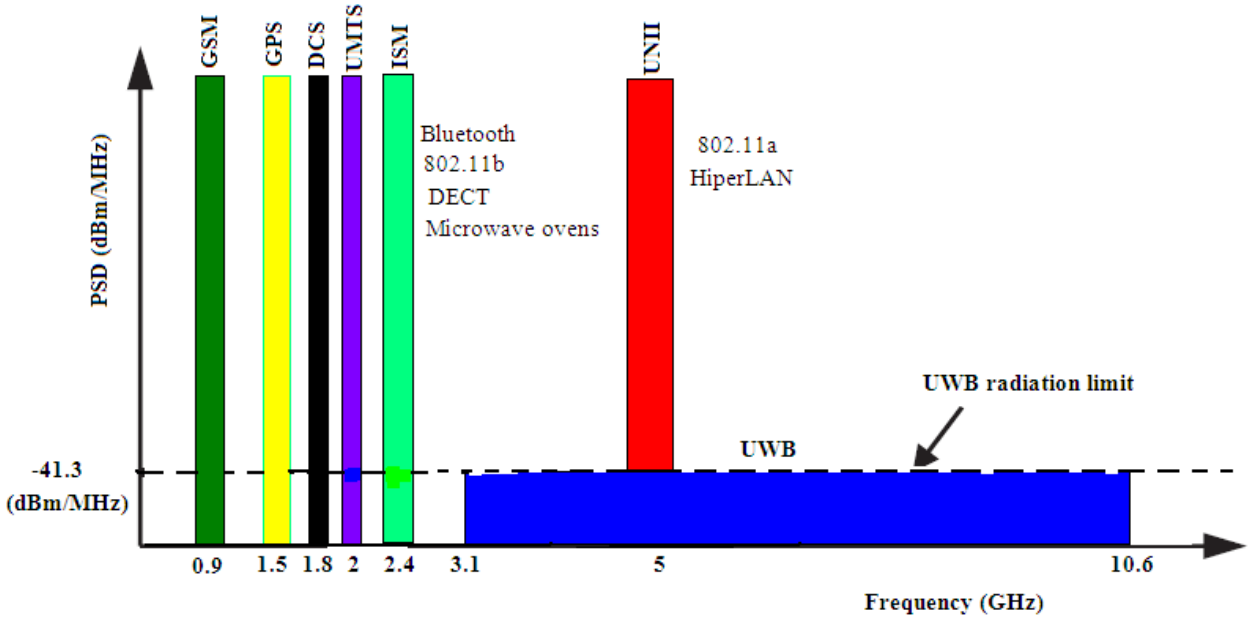

Figure 1.1: The spectrum of the UWB signal versus conventional signals

To avoid interference with existing communication systems, various regions of the spectrum should have different allowed power spectral densities. The Federal Communications Commission (FCC) has assigned the effective isotropic radiated power (EIRP) allowed for each frequency band [19].

The FCC mask depicts the allowed power spectral densities for specific frequencies. Figure 1.2 illustrates the FCC radiation limits for the indoor UWB communication system. The level –41.3 dBm/MHz, in the frequency range of 3.1–10.6 GHz, is set to limit interference to existing communication systems, and to protect the existing radio services. This level (–41.3 dBm/MHz),

is 75 nW/MHz which is in fact at the unintentional radiation level of television sets or monitors (FCC part 15 limit). For the UWB communications the FCC has assigned two FCC masks for the indoor and outdoor UWB devices. For the indoor and outdoor UWB communications, the FCC radiation limits in the frequency range of 3.1–10.6 GHz are alike. While for the 1.61–3.1 GHz frequency range the outdoor radiation limit is 10 dB lower than the indoor mask. The FCC mask for the outdoor UWB communication devices is shown in Figure 1.2. It should be noted that according to the FCC rules, the outdoor UWB communications is confined to handheld devices with no use of fixed infrastructure.

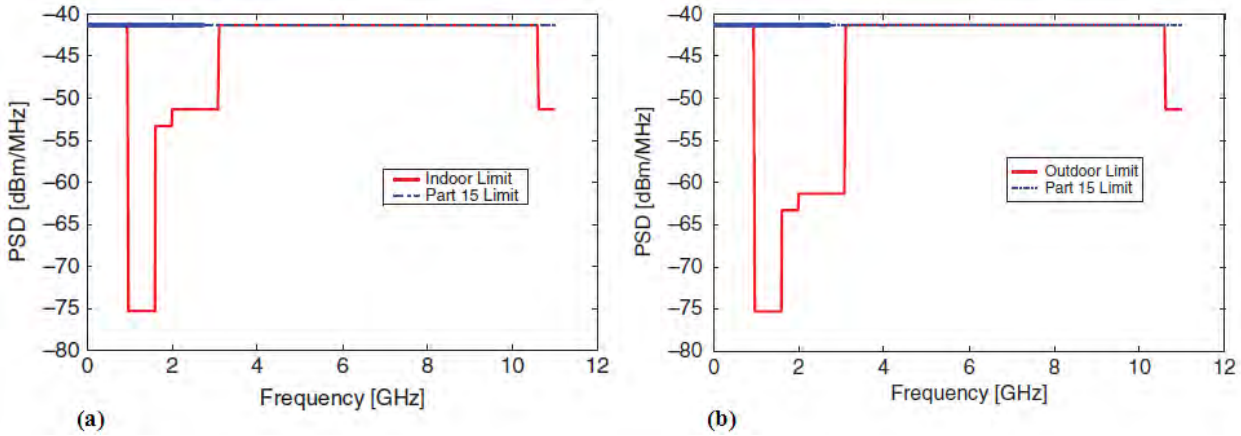

Figure 1.2: FCC Emission limits for indoor and outdoor UWB communications **a**) Indoor **b**) Outdoor

1.1.3. Advantages of UWB

The nature of the short-duration pulses used in UWB technology offers several advantages over narrowband communications systems [48]. The main advantages of UWB technology are:

- ***High channel capacity:*** The extremely large bandwidth occupied by UWB gives the potential of very high theoretical capacity, yielding very high data rates. This can be seen by considering *Shannon's capacity equation* [3], given by:

$$C = Blog\left(1 + \frac{S}{N}\right) \tag{1.2}$$

where C is the maximum channel capacity (bits/s), B the signal bandwidth (Hz), S the signal power (W) and N the noise power (W).

Shannon's equation shows that capacity is directly proportional to signal bandwidth. Thus, due to its extremely large bandwidth, UWB technology has a great potential for high-speed wireless communications.

While current chipsets are continually being improved, most UWB communication applications are targeting the range of 100–500 Mbps [41], which is roughly the equivalent of wired Ethernet to USB 2.0. It is significant that this data rate is 100 to 500 times the speed of Bluetooth, around 50 times the speed of the 802.11b, or 10 times the 802.11a WLAN standards.

As can be seen in Table 1.1 the current target data rate for indoor wireless UWB transmission is between 110 Mbps and 480 Mbps. This is fast compared with current wireless and wired standards. In fact, the speed of transmission is currently being standardized into three different speeds: 110 Mbps with a minimum transmission distance of 10 m; 200 Mbps with a minimum transmission distance of 4 m; and 480 Mbps with less than 1m distance.

The reasons for these particular distances lie mostly with different applications. For example, 10 m will cover an average room and may be suitable for wireless connectivity for home theater. A distance of less than 4 m will cover the distance between appliances, such as a home server and a television. A distance of less than 1 m will cover the appliances around a personal computer.

Table 1.1: Comparison of UWB bit rate with other wired and wireless standards

Wireless standard	Maximum speed [Mbps]
UWB (1m minimum), USB 2.0	480
UWB (4m minimum)	200
UWB (10m minimum)	110
Fast Ethernet	90
802.11a	54
802.11g	20
802.11b	11
Ethernet	10
Bluetooth	1

- ***Low power consumption:*** With proper engineering design the resultant power consumption of UWB can be quite low. As with any technology, power consumption is expected to decrease as more efficient circuits are designed and more signal processing is done on smaller chips at lower operating voltages. The current target for power consumption of UWB chipsets is less than 100 mW.
- ***High spacial and low spectral capacities:*** Another basic property of UWB systems is their high *spatial capacity*, measured in bits per second per square meter [bps/m2] [34]. Spatial capacity is a relatively recent term, and its use stems from the interest in even higher data rates, even over extremely short distances. Spatial capacity can be calculated as the maximum data rate of a system divided by the area over which that system can transmit. The transmission area can be calculated from the circular area, assuming a transmitter in the center. However, in practice a rule of thumb is to use the square of the maximum transmission distance.

$$Spacial\ capacity\left(\frac{bps}{m^2}\right) = \frac{Maximum\ data\ rate\ (bps)}{Transmission\ area(m^2)} \tag{1.3}$$

Table 1.2: Comparison of the spatial capacity of various indoor wireless systems

Communication system	Maximum data rate (Mbps)	Transmission distance (m)	Spacial capacity (kbps/m^2)	Spectral capacity (bps/Hz)
UWB	≥100	10	≥318.3	≤0.013
IEEE 802.11a	54	50	6.9	2.7
Bluetooth	1	10	3.2	0.012
IEEE 802.11b	11	100	0.350	0.1317

For narrowband systems the most popular measure of capacity has been *spectral capacity*, measured in bits per second per hertz (bps/Hz), because the spectrum has been the most limited resource. Power has generally only been limited by safety and commercial reasons, such as the battery life of mobile devices.

$$Spectral\ capacity\ \left(\frac{bps}{Hz}\right) = \frac{Maximum\ data\ rate\ (bps)}{Bandwidth(Hz)} \quad (1.4)$$

For UWB systems, which operate in other licensed spectra, the power has to be kept very low. This is compensated for by the use of extremely large bandwidths. Using the traditional measure of spectral capacity [bits/Hz], UWB has very low spectral capacity compared with existing systems.

- ***Coexistence with other services**:* UWB systems have low power spectral density that allows them to coexist with other services such as cellular systems, wireless local area networks (WLAN), global positioning systems (GPS), etc…
- ***Fading robustness**:* Multipath fading occurs when modulated signals arrive at the receiver from different paths. Combining these signals at the receiver can result in signal distortion. The ultra-short duration of UWB waveforms gives rise to a fine resolution of reflected pulses at the receiver. As a result, UWB technology is capable of resolving multipath components and is rich in multipath diversity. Thus, UWB systems are immune to multipath fading.
- ***Security**:* Since UWB systems operate below the noise floor, they are inherently covert and extremely difficult for unintended users to detect.
- ***Superior penetration properties**:* UWB systems can penetrate obstacles and thus operate under both line-of-sight (LOS) and non-LOS (NLOS) conditions.
- ***High precision ranging**:* UWB systems have good time-domain resolution and can promise sub-centimeter resolution capability for location and tracking applications.
- ***Simple transceiver architecture**:* transmission of low-powered pulses eliminates the need for a power amplifier (PA) in UWB transmitters and since UWB transmission is carrierless, there is no need for mixers and local oscillators to translate the carrier frequency to the required frequency band. This in turn avoids the need for a carrier recovery stage at the receiver end.

1.1.4. Applications of UWB

UWB technology can enable a wide variety of applications in wireless communications, networking, radar imaging, and localization systems. For wireless communications the use of

UWB technology under the FCC guidelines [19] offers significant potential for the deployment of two basic communications systems:

- ***High-data-rate short-range communications***: The high-data-rate wireless personal area networks (WPANs) can be defined as networks with a medium density of active devices per room (5 to 10) transmitting at data rates ranging from 100 to 500 Mbps within a distance of 20 m. The ultra-wide bandwidth of UWB enables various WPAN applications, such as high-speed wireless universal serial bus (WUSB) connectivity for personal computers (PCs) and PC peripherals, high-quality real time video and audio transmission, file exchange among storage systems, and cable replacement for home entertainment systems.

  The IEEE 802.15.3 standard task group has established the 802.15.3a study group [TG3a] to define a new physical layer concept for high-data-rate WPAN applications. A major goal of this study group is to standardize UWB wireless radios for indoor WPAN transmissions. The goal for the IEEE 802.15.3a standard is to provide a higher-speed physical layer for the existing approved 802.15.3 standard for applications that involve imaging and multimedia. The work of the 802.15.3a study group includes standardizing the channel model to be used for UWB system evaluation.
- ***Low-data-rate and long range communications***: Under the low-rate operation mode, UWB technology could be beneficial and potentially useful in sensor, positioning, and identification networks over relatively long range. A sensor network comprises a large number of nodes spread over a geographical area to be monitored. Depending on the specific application, the sensor nodes can be static or mobile. Key requirements for sensor networks operating in challenging environments include low cost, low powers, and multi-functionality. With its unique properties of low complexity, low cost, and low power, UWB technology is well suited to sensor network applications [44]. Moreover, due to the fine time resolution of UWB signals UWB-based sensing has the potential to improve the resolution of conventional proximity and motion sensors. The low-rate transmission, combined with accurate location tracking capabilities, offers an operational mode known as *low-data-rate and location tracking*.

  The IEEE also established the 802.15.4 study group to define a new physical layer concept for low-data-rate applications utilizing UWB technology at the air interface. The study group

addressed new applications which require only moderate data throughput but long battery life, such as low-rate wireless personal area networks, sensors, and small networks.

1.2. Problem Statement

Due to its potential advantages and applications, UWB technology for wireless communication has been the subject of extensive research in recent years. Researchers are nowadays devoting considerable efforts and resources to develop robust, reliable and flexible wireless communication systems using UWB technology. However, there are many challenges that have not yet been thoroughly examined and need to be carefully studied to ensure the success of this technology in the wireless communication industry. The main challenges that still require a great deal of investigation include: optimum transmitter and receiver design, narrow band interference (NBI) cancellation from other coexisting systems, multiple access interference cancellation, time synchronization for short-duration pulses, accurate channel modeling and estimation, etc…

Being one of the main components for reliable communication, many receiver types have been proposed for UWB wireless communication systems. But due to their better bit error rate (BER) performance in multipath fading environment, RAKE and adaptive MMSE receivers are the best choices for this technology and most commonly found in different UWB literatures. Infact, these two receiver types have different bit error rate (BER) performance for different system parameters. Thus, in order to select the best receiver for a certain application, it is very essential to investigate its bit error rate (BER) performance for different system parameters including transmitted signal formats, number of users, channel types, adaptive algorithms, etc…

In this thesis, bit error rate (BER) performance of RAKE and adaptive MMSE receivers has been evaluated thoroughly based on the above parameters. Specifically, BER performance of RAKE receiver for different bit repetition code lengths and selective combining (SC) technique, BER performance of adaptive MMSE receiver using LMS adaptive algorithm and BER performance comparison of RAKE and adaptive MMSE receivers have not been covered in previous literature and are the main focus for this thesis.

1.3. Objective of the Thesis

1.3.1. General Objective

The general objective of this thesis is to evaluate the bit error rate (BER) performance of RAKE and adaptive MMSE receivers for UWB wireless communication systems.

1.3.2. Specific Objectives

The specific and detailed objectives of this thesis are described as follows.

- To analyze and compare different modulation techniques and multiple-access schemes for UWB wireless communication systems.
- To evaluate bit error rate (BER) performance of Rake receiver on standard IEEE 802.15.3a channel model for different RAKE receiver types (ARAKE, PRAKE, SRAKE), number of RAKE fingers, RAKE combining techniques (MRC, EGC, SC), transmitted signal formats (TH-PAM, TH-OOK, TH-PPM, TH-BPSK, DS-BPSK) and bit repetition code lengths.
- To evaluate bit error rate (BER) performance of adaptive MMSE receiver on standard IEEE 802.15.3a channel model for different adaptive algorithms (LMS, NLMS, RLS).
- To evaluate bit error rate (BER) performance of adaptive MMSE receiver for different number of users (single-user, multi-user) by considering the effect of multiple access interference (MAI).
- To compare bit error rate (BER) performance of RAKE and adaptive MMSE receivers for single user scenario.

1.4. Literature Review

So far many researches have been conducted on different aspects UWB wireless communication systems, in general, and on RAKE and adaptive MMSE receivers, in particular. A short summary of some of the researches are reviewed here.

X. Chen and S. Kiaei [1] investigated several candidate monocycle (narrow pulse) shapes, their spectrum characteristics and BER performance in AWGN using pulse position modulation (PPM). Their performances in the fading multipath channel are also investigated.

I. Guvenc and H. Arslan [5] reviewed various modulation options for ultra-wideband (UWB) systems and evaluated their performances under practical conditions such as multipath, multiple-access interference (MAI), narrowband interference (NBl) and timing jitter. In this paper, it is shown that BPSK has the best performance and the performance PPM degrades in multipath and multi-user environments since symbols occupy larger time durations. In addition, it is shown that OOK and M-ary PAM are more susceptible against timing jitter compared to other modulations.

G. Durisi and S. Benedetto [8] evaluated BER performance of UWB systems employing TH and DS multiaccess techniques in presence of multiuser and narrowband interference under multipath channel analytically. In this paper, TH is shown to be as robust as DS in presence of strong narrowband and multiuser interference and dense multipath channel. But only PAM modulation technique is used for system analysis and evaluation and in this thesis work this is extended to other possible UWB modulation techniques.

M. G. Khan, et al. [2] evaluated the BER performance of RAKE receivers operating in a non line-of-sight (NLOS) scenario industrial environments using measured channels. In this paper, measured channels in a medium-sized industrial environment and a standard IEEE 802.15.4a channel model are used and only TH-BPSK-UWB transmitted signal format is considered for BER performance evaluation. The performance of PRAKE and SRAKE receivers is evaluated in terms of uncoded bit-error-rate (BER) using different number of RAKE fingers. The performance of maximal ratio combining (MRC) and equal gain combining (EGC) is compared for the RAKE receiver assuming perfect knowledge of the channel state. This paper illustrated that SRAKE receiver has better BER performance compared to PRAKE receiver for the same number of fingers and MRC combining technique performs better compared to EGC. However, in my thesis work thesis work, ARAKE receiver, selective combining (SC), bit repletion coding and other possible UWB modulation schemes are also considered for performance comparison in addition to the above parameters and the standard IEEE 802.15.3a channel model is used.

A. Rajeswaran, et al. [6] studied the BER performance of RAKE receiver in a realistic channel model that is based on an extensive set of indoor channel measurements with different number of RAKE taps. In this paper, it is shown that the RAKE receiver contributes to a mitigation of the ISI. In particular, at low input SNR values and small number of RAKE taps, it is shown that employing additional RAKE taps for energy capture is more important to overall system

performance than employing equalization to combat the ISI. The performance of the RAKE with some realistic channel estimation errors is also studied.

D. Cassioli, et al. [9] presented the performance of PRAKE and SRAKE receivers under a statistical tapped-delay-line channel model that is based on extensive measurement campaigns, and reflects both small-scale and large scale variations of the channel. In this paper, it is shown that SRAKE receiver has in general better BER performance than PRAKE receiver for the same number of RAKE fingers.

L. Jiabin and L. Zhonghua [4] analyzed the BER performance of adaptive MMSE receiver using RLS adaptive algorithm for DS-BPSK-UWB transmitted signal format under standard 802.15.3a UWB indoor channel model for different number of users. In this paper, it is shown that nearly without loss of BER performance compared with the traditional Rake receiver scheme, the adaptive MMSE receiver requires no channel estimation and, therefore, is simpler in structure and easier for implementation and with a relatively higher data rate. In my thesis work, BER performance of adaptive MMSE receiver using LMS and NLMS algorithms is also analyzed in addition to the RLS algorithm used in this paper.

1.5. Methodology

The methodology used in conducting this thesis work can be summarized into three basic steps. The major tasks performed in each step are described as follows.

Literature review: In this step, the issues and concepts that are closely related to this thesis work have been thoroughly studied in order to acquire a deep understanding and knowledge of the relevant areas and where the problem lies. Different literatures (books, standard journals, research papers, class lecture notes, research publications and other information available on the Internet) that are conducted on UWB signal generation, modulation options, multiple access techniques, RAKE and adaptive MMSE receiver modeling and analysis, adaptive algorithms and combining techniques have been reviewed.

System Modeling and Analysis: In this step, the general UWB system for wireless communication including the transmitter, transmission channel, RAKE and adaptive MMSE receivers are modeled and mathematically analyzed.

Simulation and Evaluation of Results: In this final step, the bit error rate (BER) performance of both RAKE and adaptive MMSE receivers for different system parameters has been simulated according to the given system model using MATLAB software and conclusions are drawn based on the results.

1.6. Organization of the Thesis

This thesis has been divided into 6 chapters. A general overview of UWB wireless communication systems and literature survey of some selected papers on RAKE and adaptive MMSE receivers is covered in chapter 1. Chapter 2 presents the general system modeling for UWB wireless communications. UWB Pulse generation, modulation options, and multiple access techniques are discussed. An overview UWB channels, in general, and basic feature of standard IEEE 802.15.3a channel model, in particular, is presented. Chapter 3 deals with the RAKE receiver. The general structure of RAKE receiver is defined and different RAKE receiver types are discussed. The most common RAKE combining techniques are also explained. Chapter 4 provides a study of adaptive MMSE receiver. The general structure of adaptive MMSE receiver is defined and different adaptive algorithms are also discussed here. Chapter 5 presents the simulation results of the two receivers for different system parameters and discussion of results. Chapter 6 contains the conclusion of the thesis and some suggestions for future work. The reference materials that are used in this thesis directly follow the conclusion and suggestion section.

Chapter 2

UWB Wireless Communication System Modeling

2.1. Transmitted Signal Model

So far, several UWB transmission techniques have been proposed in the literature. These techniques can be categorized into two major groups: *single-band* and *multi-band* UWB. The single-band approaches, also referred to as carrier-free and impulse communications, are implemented by direct modulation of information into a sequence of impulse like waveforms which occupy the available bandwidth of 7.5 GHz. Multi-band approaches, on the other hand, divide the available UWB bandwidth into smaller sub-bands, each with a bandwidth greater than 500 MHz, to comply with the FCC's definition of UWB signals. This thesis deals with only single-band transmission approaches.

Figure 2.1 presents the general block diagram of UWB wireless communication systems. The diagram consists of three main blocks, *transmitter*, *channel* and *receiver*, which are also common for any communication system.

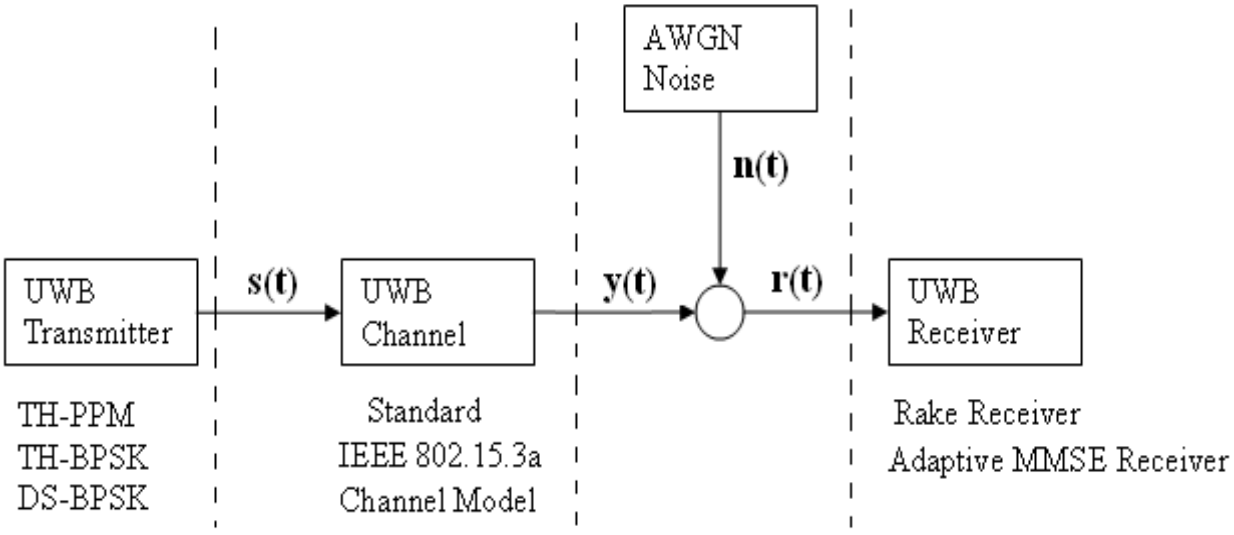

Figure 2.1: General block diagram for UWB wireless communication systems

In this thesis work, different transmitted signal formats are generated by the transmitter and the standard IEEE 802.15.3a channel model is considered. Although different receiver types are proposed for UWB wireless communication systems by many researchers, especial attention is

given to RAKE and adaptive MMSE receivers due to their better performance and interference cancellation characteristics in multipath fading environment. Thus, in this thesis, only RAKE and adaptive MMSE receivers are considered and their BER performance is examined thoroughly for different system parameters.

Figure 2.2 illustrates the detail structure of a typical UWB transmitter that transmits different signal formats for UWB wireless communication systems.

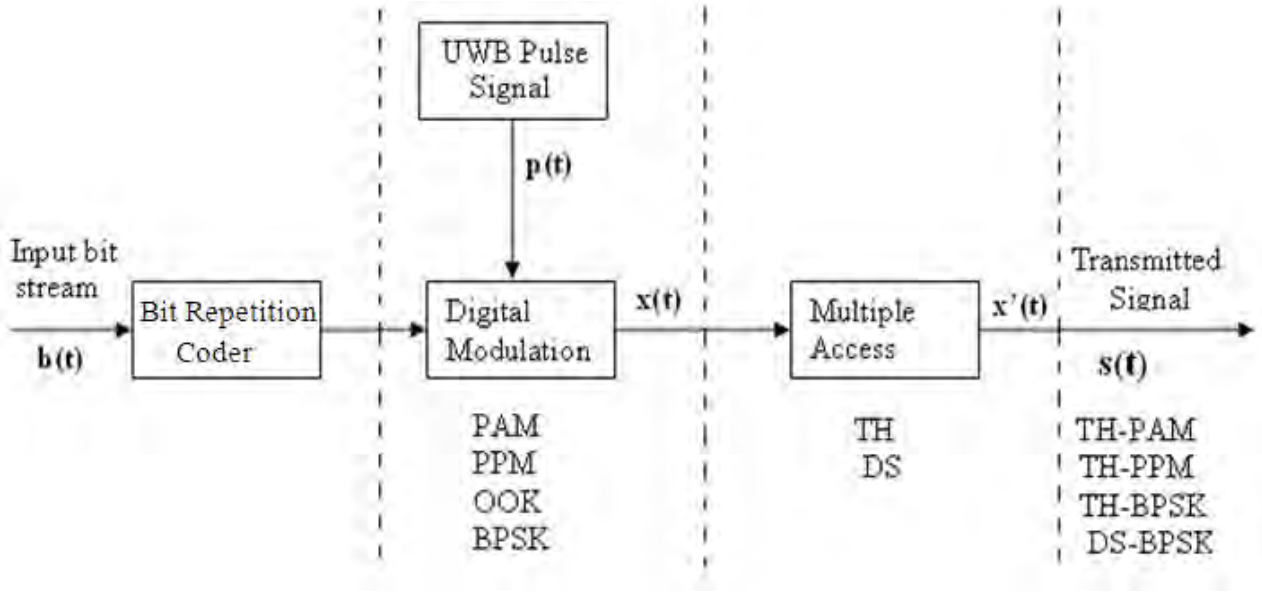

Figure 2.2: Transmitter block diagram for UWB wireless communication systems

Pulse generation, data modulation and multiple access are the three main tasks that are performed at the transmitter end of a typical UWB communication system and each task is discussed in detail in the next subsections.

2.1.1. UWB Signal Generation

The first step in a radio communication link involves the generation of a suitable signal, which is then modulated with desired information before transmission through the communication channel. Several waveforms have been proposed in the literature for UWB wireless communication systems such as Gaussian, Rayleigh, Laplacian, cubic, and Hermitian pulses [40]. The Gaussian pulse is the most common one since its shape can be easily modified by modifying its shape factor, infinite waveforms can be obtained by differentiating the original pulse and it can be generated by pulse generators more easily. Thus, a detail description of only Gaussian

pulses is presented here. Gaussian pulses are waveforms whose mathematical definition is similar to the normal Gaussian function. Mathematical expressions for the Gaussian pulse and its higher order derivatives are given in [22, 24, 28, 40]. The zero-order Gaussian pulse is given by

$$g_0(t) = A_0 e^{\left(-\frac{t^2}{2\sigma^2}\right)} = A_0 e^{\left(-2\pi\frac{t^2}{\tau^2}\right)} \tag{2.1}$$

where $\sigma = \frac{\tau}{2\sqrt{\pi}}$

A_0 , σ and τ represent the amplitude constant, spread of the Gaussian pulse and the pulse shaping factor respectively.

The frequency domain representation of the zero-order Gaussian pulse is given by:

$$G_0(f) = A_0\sigma\sqrt{2\pi}e^{(-2\pi^2\sigma^2 f^2)} = A_0\frac{\tau}{\sqrt{2}}e^{\left(-\frac{\pi}{2}\tau^2 f^2\right)} \tag{2.2}$$

Usually higher derivatives of Gaussian pulses are more popular for the UWB transmission. This is mainly due to lower DC value of the pulses as the order of the derivative increases. As antennas are not efficient at DC, it is preferable to use derivatives of Gaussian pulses having smaller DC components. The nth derivative of Gaussian pulse can be obtained recursively from the following expression:

$$g_n(t) = -\frac{n-1}{\sigma^2}g_{n-2}(t) - \frac{t}{\sigma^2}g_{n-1}(t) \tag{2.3}$$

The frequency domain representation of the nth derivative Gaussian pulse can be obtained from

$$G_n(f) = A_n(j2\pi f)^n G_0(f) \tag{2.4}$$

Figure 2.3 shows the time domain graphical representation of the zero-order Gaussian pulse and the its first five higher order derivatives.

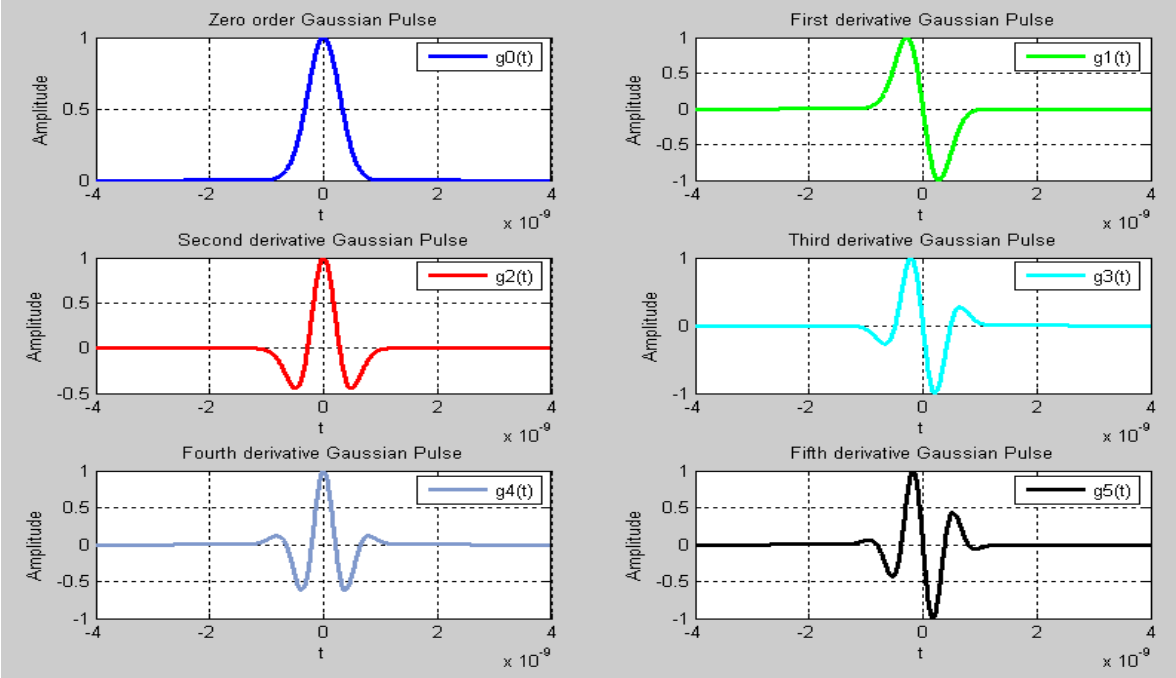

Figure 2.3: Time-domain representation of Gaussian pulse and its higher order derivatives

In this thesis, the second-order Gaussian pulse is used. The mathematical representation for this pulse is given

$$g_2(t) = \frac{A_2}{\sigma^2}\left(1 - \frac{t^2}{\sigma^2}\right)e^{\left(-\frac{t^2}{2\sigma^2}\right)} = \frac{A_2(4\pi)}{\tau^2}\left(1 - 4\pi\frac{t^2}{\tau^2}\right)e^{\left(-2\pi\frac{t^2}{\tau^2}\right)} \tag{2.5}$$

The frequency domain representation of the second-order Gaussian pulse can be expressed as

$$G_2(f) = A_2(j2\pi f)^2 G_0(f) \tag{2.6}$$

Figure 2.4 illustrates the time and frequency domain graphical representation of the second-order Gaussian pulse.

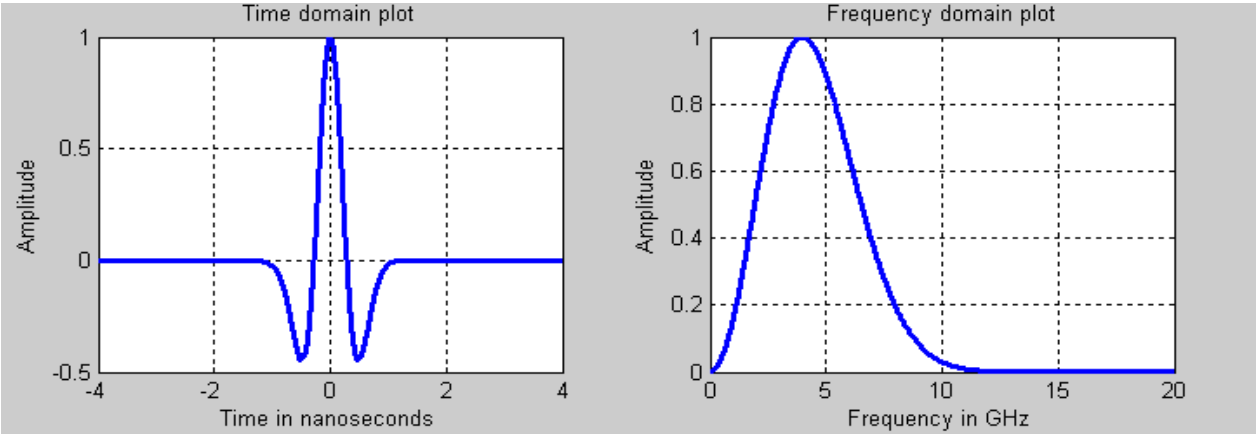

Figure 2.4: Graph of second-order Gaussian pulse in time and frequency domain

In order to minimize intersymbol interference (ISI) between consecutive trains of pulses, UWB signals are usually transmitted with very low duty cycle. The duty cycle of UWB pulses is defined by

$$duty - cycle = \frac{T_w}{T_f} \tag{2.7}$$

where T_w is the pulse width (pulse duration) and T_f is the pulse repetition time (frame interval).

Figure 2.5 depicts a sequence of second order Gaussian pulses with a low duty cycle. Typically, the frame interval T_f is 100 or 1000 times longer than the pulse width T_w in order to minimize the ISI in practical UWB wireless communication systems.

Figure 2.5: A sequence of second order Gaussian pulse train with low duty cycle

2.1.2. UWB Modulation Options

A major challenge when designing UWB systems is the selection of the appropriate modulation scheme. Data rate, transceiver complexity, BER performance, spectral characteristics of the transmitted signal, and robustness against impairments and interference are all related with the employed modulation type. Thus, determining the right modulation for a given application is

crucial in UWB system design. For pulsed UWB systems, the widely used forms of modulation schemes include on-off keying (OOK), pulse amplitude modulation (PAM), pulse position modulation (PPM) and binary phase shift keying (BPSK) [5, 29, 33].

2.1.2.1. On-Off Keying (OOK)

On-off keying (OOK) is the simplest form of pulse modulation, in which the transmission of a pulse represents a data bit 1 and its absence represents a data bit 0. An OOK signal can be modeled as

$$x(t) = \sum_{j=-\infty}^{\infty} m_j \, g_2\left(t - jT_f\right) \tag{2.8}$$

Where:

$m_j \in [0, 1]$ is the amplitude of the j[th] pulse

$g_2(t)$ is the second derivative Gaussian pulse

T_f is the pulse repetition period

The main advantages of OOK are simplicity and low implementation cost. The OOK transmitter is quite uncomplicated; a simple RF switch can be turned on and off to represent data. This way, OOK modulation allows the transmitter to idle while transmitting a bit 0 and thus save power. The detection of OOK-modulated pulses is typically done with a no coherent energy detector receiver, although classical matched filter (CMF) receivers can also be used.

Despite the simplicity of OOK transmitters, this modulation scheme has several disadvantages in UWB systems. OOK is highly sensitive to noise and interference: an unwanted signal can be detected as a false data bit 1. Therefore, OOK is not a popular modulation technique for multiple-access communications channels.

Figure 2.6: On-off keying (OOK) modulated signal

2.1.2.2. Pulse Amplitude Modulation (PAM)

The information in a PAM signal is conveyed in the amplitude of pulses. Specifically, an *M*-ary PAM signal comprises a sequence of modulated pulses with *M* different amplitude levels. The PAM signal can be modeled as

$$x(t) = \sum_{j=-\infty}^{\infty} a_{mj}\, g_2\left(t - jT_f\right) \tag{2.9}$$

Where:

a_{mj} is the amplitude of the j[th] pulse

$g_2(t)$ is the second derivative Gaussian pulse

T_f is the pulse repetition period

PAM generation is simple because it requires pulses with only one polarity to represent data. Pulses modulated with PAM can be detected with an energy detector receiver or a classical matched filter (CMF) receiver. Although PAM pulses are less sensitive to noise than OOK-modulated pulses, attenuation in wireless channels can convert them to the OOK case. Furthermore, because of the periodicity of transmitted pulses, some discrete lines will be present on the power spectral density (PSD) of PAM pulses. These discrete lines can cause harmful interference to other narrowband and wideband signals sharing the frequency spectrum with UWB systems.

Figure 2.7: Four-ary Pulse Amplitude Modulation (PAM) modulated signal

2.1.2.3. Pulse Position Modulation (PPM)

In this technique signals are pseudo randomly encoded based on the position of the transmitted pulse trains by shifting the pulses in a predefined window in time. A PPM represents a data bit 0 by a pulse with no shift with respect to a specific reference point in time and it represents a data

bit 1 by a shifted pulse with respect to a specific reference point in time. The *M*-ary PPM signal can be modeled as

$$x(t) = \sum_{j=-\infty}^{\infty} g_2\ (t - jT_f - m_j\ T_d) \tag{2.10}$$

Where:

m_j is the j[th] pulse M-ary symbol

$g_2(t)$ is the second derivative Gaussian pulse

T_f is the pulse repetition period

T_d is the modulation delay

Compared to OOK and PAM pulses, PPM signals are more immune to false detection. This is because the pulses that represent the data bits in PPM have the same amplitude, so the probability of detecting a false data bit is reduced. However, they are vulnerable to catastrophic collisions that are caused by multiple-access channels.

Moreover, the pseudorandom code sequence of the pulse positions reduces the discrete lines on the power spectral density of the PPM signal more than those of the PAM signal.

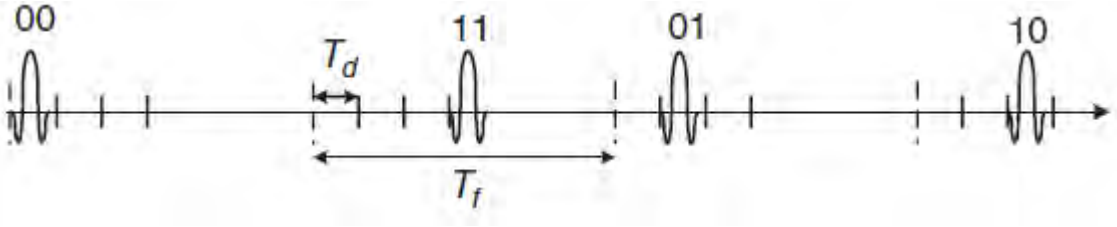

Figure 2.8: Four-ary pulse position modulated (PPM) signal

2.1.2.4. Binary Phase Shift Keying (BPSK)

In binary phase shift keying (BPSK), the polarity of the pulse changes to represent digital data bits. A pulse with positive polarity represents a digital bit 1 where as a pulse with negative polarity corresponds to a bit 0. A BPSK signal can be modeled as

$$x(t) = \sum_{j=-\infty}^{\infty} d_j g_2\ (t - jT_f) \tag{2.11}$$

Where:

$d_j \in [-1, 1]$ is the polarity of the modulated pulse

$g_2(t)$ is the second derivative Gaussian pulse

T_f is the pulse repetition period

This type of modulation scheme is less susceptible to distortion because the difference between the two pulse levels is twice the pulse amplitude. Another advantage of BPSK is that the change in polarity can remove the discrete spectral lines in the pulse's PSD, because changing the polarity of pulses produces a zero mean. However, this modulation scheme results in more complexity in the physical implementation of the transmitter: It requires one transmitter to generate positive pulses and another transmitter to generate negative pulses.

Figure 2.9: Binary Phase Shift Keying (BPSK) signal

2.1.3. UWB Multiple Access Schemes

In single-band UWB systems, multiple users share a single UWB spectrum simultaneously. To accommodate these multiple users, proper multiple access techniques are necessary. Two commonly used multiple techniques in single-band UWB systems are time-hopping (TH) and direct-sequence (DS) spreading techniques. In TH-based systems [13, 29, 33], the information is sent with a time offset for each pulse determined by the TH sequence. In DS spreading systems [30, 39], the data are carried in multiple pulses whose amplitudes are based on a certain spreading code. TH and DS spreading codes both provide robustness against multiuser interference. The performance comparisons of TH and DS schemes for single-antenna systems have been studied [18, 45] and it has been shown that TH-UWB systems are suitable in theory and analysis but are seldom used in practice due to the need for perfect time synchronization between the transmitter and the receiver**.** On the other hand, DS-UWB has been shown to be a promising scheme for single-carrier UWB communications.

2.1.3.1. Time Hoping (TH)

TH-UWB utilizes low-duty-cycle pulses, where the time spreading between the pulses is used to provide time multiplexing of users. Basically, each frame interval duration is divided into multiple smaller segments and only one of these segments carries the user's transmitted monocycle. A unique code, also referred to as a *TH sequence*, is assigned to each user to specify which segment in each frame interval is used for transmission. In TH-UWB systems, the frame interval T_f is divided into N_c segments of T_c seconds such that $N_c T_c \leq T_f$. The TH sequence is denoted by C_j, $0 \leq C_j \leq N_c - 1$. It provides an additional time shift of $C_j T_c$ seconds to the j^{th} monocycle to allow multiple access without catastrophic collisions. The signal for TH-UWB system can be modeled as

$$x'(t) = \sum_{j=-\infty}^{\infty} g_2(t - jT_f - C_j T_c) \tag{2.12}$$

In a synchronized network, an orthogonal TH sequence that satisfies $C_j^k \neq C_j^{k'}$ for all j's and for any two users $k \neq k'$ can be adopted to minimize interference between the users. The performance of synchronous multiple access systems using various TH sequences such as the Gold sequence and a simulated annealing code has been studied in [43]. For an asynchronous system, the choice of orthogonal TH sequence does not guarantee collision-free transmission [18]. By combining the TH technique with the various modulation options discussed in section 2.1.2, different transmitted signal formats can be generated. The transmitted signal formats using PAM, PPM and BPSK modulation schemes can be modeled as follows.

- TH-PAM-UWB transmitted signal format:

$$s(t) = \sum_{j=-\infty}^{\infty} a_{mj}\, g_2\big(t - jT_f - C_j T_c\big) \tag{2.13}$$

- TH-PPM-UWB transmitted signal format:

$$s(t) = \sum_{j=-\infty}^{\infty} d_j\, g_2\big(t - jT_f - C_j T_c\big) \tag{2.14}$$

- TH-BPSK-UWB transmitted signal format:

$$s(t) = \sum_{j=-\infty}^{\infty} g_2\left(t - jT_f - C_jT_c - m_jT_d\right) \tag{2.15}$$

2.1.3.2. Direct Sequence (DS)

DS-UWB employs a train of high-duty-cycle pulses whose polarities follow pseudorandom code sequences. Specifically, each user in the system is assigned a pseudorandom sequence that controls pseudorandom inversions of the UWB pulse train.

In a DS-UWB system with BPSK modulation, the binary symbol d_j to be transmitted over the j^{th} frame interval is spread by a sequence of multiple monocycles $\left\{C(n_c)g_2(t - jT_f - n_cT_c\right\}_{n_c=0}^{N_c-1}$ whose polarities are determined by the spreading sequence $\{C(n_c)\}_{n_{c=0}}^{N_c-1}$. Such a spreading sequence is assigned uniquely to each user in a multiple access system in order to allow multiple transmissions with little interference. Similar to the TH system, an orthogonal spreading sequence such as a Gold sequence or Hadamard–Walsh code can be selected to mitigate multiple access interference in a synchronous network [39].

The DS-BPSK-UWB transmitted signal format can be described as [30, 39]

$$s(t) = \frac{1}{\sqrt{N_c}} \sum_{j=-\infty}^{\infty} d_j \sum_{n_c=0}^{N_c-1} C(n_c)g_2\left(t - jT_f - n_cT_c\right) \tag{2.16}$$

Where:

$d_j \in \{-1, 1\}$ is the modulated binary data

$C(n_c) \in \{-1, 1\}$ is the pseudorandom code or spreading sequence

$T_c \geq T_w$ represents the hop period

The factor $1/\sqrt{N_c}$ is introduced such that the sequence of N_c monocycles has unit energy.

2.2. Channel Model

Analysis and design of UWB communication systems require an accurate channel model to determine the data rate that can be achieved, to design efficient modulation and coding schemes, and to develop associated signal-processing algorithms.

2.2.1. General Overview of UWB Channel Models

Although narrowband wireless channels have been well documented in the literature, they cannot be generalized directly to UWB channels. In particular, the narrowband channels were constructed based on a signal bandwidth of less than 20 MHz. The radiation in UWB systems, on the other hand, can cover as much as 10 GHz of bandwidth. Such a large bandwidth gives rise to important differences between UWB and narrowband channels, especially with respect to the number of resolvable paths and arrival times of multipath components [10].

For a narrowband signal with a bandwidth less than the coherence bandwidth of the propagation channel, multipath components arrive continuously and severe multipath fading can be observed. When a large number of multipath components are observed at the receiver within its resolution time, the central limit theorem is commonly invoked to model the amplitude of the signal received as Rayleigh distributed. Rayleigh fading is therefore used extensively for channel models in many narrowband systems. In UWB systems, on the other hand, the number of multipath components that arrive at the receiver within the period of an ultra-short waveform is much smaller as the duration becomes shorter. Consequently, the channel fading is not as severe as that in narrowband channels and Rayleigh fading may not perfectly match the amplitude of the signal received. In addition, since the multipath components can be resolved on a very fine time duration, the time of arrival of the multipath components may not be continuous. In other words, there are empty delay bins (bins containing no energy) between the arriving multipath components.

In general, the large bandwidth of a UWB waveform considerably increases the ability of a receiver to resolve a variety of reflections in UWB channels and the signal received contains a significant number of resolvable multipath components. Additionally, due to the fine time resolution of a UWB waveform, the multipath components tend to occur in a cluster rather than in a continuum as is common for narrowband channels.

In recent years, a lot of research effort has been devoted to UWB channel modeling in order to construct channel models that are able to capture these important characteristics of UWB channels. In [23], simulation results for indoor communications using UWB signals were presented. The UWB channel is modeled as a tap-delay-line fading model and the amplitude of the multipath coefficients is characterized by Nakagami-*m* distribution. A statistical UWB channel model based on the clustering approach for multipath effects is presented in [27]. The time-domain measurement approach generally excites the channel by a short pulse and has samples of the channel response recorded at the receiver. UWB channel modeling using a frequency-domain measurement approach was presented in [20] [31]. In the frequency domain measurement approach, a vector network analyzer is used to record the channel frequency response (instead of the time-domain response). Measurements in the frequency domain are then converted to the time domain using inverse Fourier transform (IFT).

2.2.2. The Standard IEEE 802.15.3a Channel Model

As discussed above, the channel measurements in UWB systems showed multipath arrivals in clusters rather than in a continuum as is common for narrowband channels. In particular, due to the very fine resolution of UWB waveforms, different objects or walls in a room could contribute different clusters of multipath components. Therefore, reliable channel model that captures such important characteristics of UWB channel is critical for the analysis and design of UWB systems.

To have a common channel model for the evaluation of UWB communications systems, standardization groups SG3a and SG4a recently established within the IEEE 802.15 have been working to set up standard models of the UWB channel. UWB channel model for the IEEE 802.15.3a standard has been established in [10] and the model for the IEEE 802.15.4a in [11].

In this thesis, the standard IEEE 802.15.3a channel model is used for performance evaluation of RAKE and adaptive MMSE receivers since this channel model is designed for short range wireless communication systems. Thus, the main features of this channel model are described in detail as follows.

The three main indoor channel models considered to develop the standard IEEE 802.15.3a channel model are:

- ***Tap-Delay-Line Fading Model:*** A simple model for characterization of a UWB channel is the tap-delay-line fading model [10] [23], in which the signal received is a sum of the replicas of the signal transmitted, being related to the reflecting, scattering, and/or deflecting objects via which the signal propagates. Such a tap-delay-line fading model allows frequency selectivity of UWB channels to be taken into consideration. Under the tap-delay-line fading model, the channel impulse response can be described as [3]

$$h(t) = \sum_{i=0}^{L-1} \alpha_i \delta(t - \tau_i) \tag{9.17}$$

where α_i is the multipath gain coefficient of the i^{th} path, L denotes the number of resolvable multipath components, and τ_i represents the path delay of the i^{th} path.

- **Δ*-K Model:*** The Δ–*K* model was introduced for the outdoor environment, and popularized for the indoor scenario by [35]. The Δ–*K* model defines two states: state A, where the arrival rate of paths is λ, and state B, where the rate is $K\lambda$. The model starts in state A. If a path arrives at time t, a transition is made to state B for a minimum of time λ. If no path arrives during that time, the model reverts to state A; otherwise, it remains in state B. The Δ–*K* model was used for UWB channels in [17] [25].
- ***Saleh–Valenzuela Model:*** The Saleh–Valenzuela (S-V) model [15] was introduced for a wideband indoor channel. In the S-V model multipath arrivals are grouped into two different categories: a cluster arrival and a ray arrival within a cluster. This model requires four main parameters: the cluster arrival rate, the ray arrival rate within a cluster, the cluster decay factor, and the ray decay factor. The channel impulse response of the S-V model is modeled by

$$h(t) = \sum_{c=0}^{C} \sum_{i=0}^{L} \alpha_{ci} \delta(t - T_c - \tau_{ci}) \tag{2.18}$$

where α_{ci} denotes the gain of the i^{th} multipath component in the c^{th} cluster, C is the total number of clusters, and L is the total number of rays within each cluster

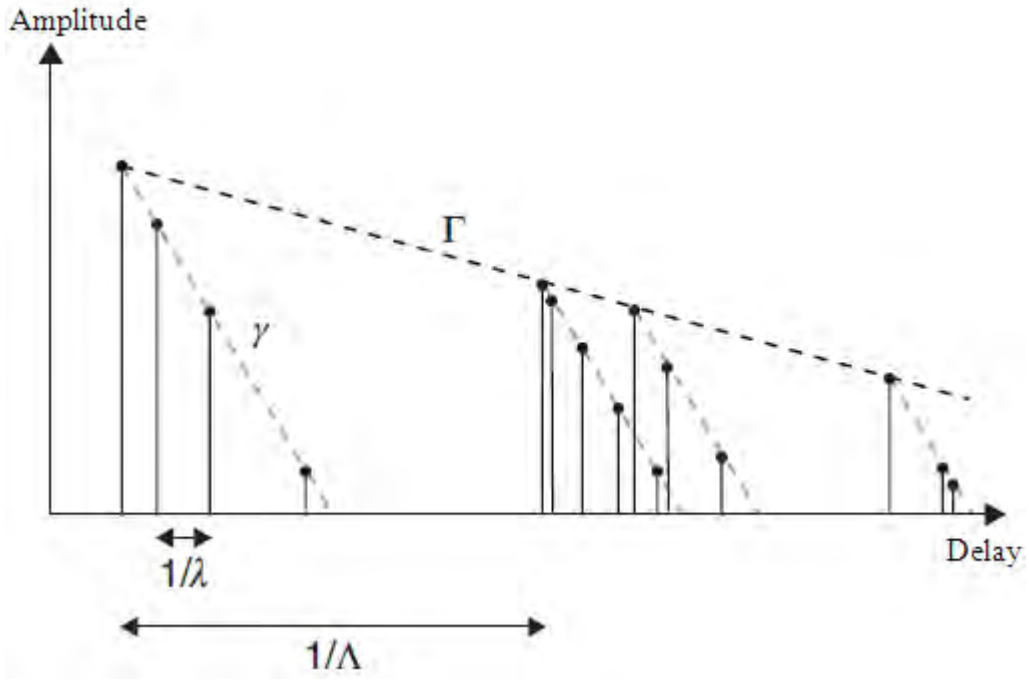

Figure 2.10: Principle of the Saleh–Valenzuela fading model

The path loss, shadowing, and small-scale fading models of the standard IEEE 802.15.3a UWB channel model are provided below.

- ***Path loss**:* The path loss specified in the standard is based on free-space path loss, with the center frequency *fc* given by $f_c = \sqrt{f_L f_H}$, where f_L and f_H are obtained at the −10dB edges of the waveform spectrum
- ***Shadowing**:* The shadowing is assumed log-normally distributed with standard deviation of 3 dB [i.e., the shadowing is $X\sigma$ [dB] ~ $N(0, \sigma 2)$, with a σ value of 3 dB].
- ***Small-scale fading:*** The small-scale fading adopted in the IEEE 802.15.3a standard is based on the S-V model. Although the path amplitude $|\alpha_{ci}|$ may follow the lognormal distribution [10], the Nakagami distribution [23], or the Rayleigh distribution [27], the lognormal distribution is adopted in the standard.

The standard IEEE 802.15.3a channel model defined four channel types for UWB applications, namely CM1, CM2, CM3 and CM4 for different types of indoor measurement environments. CM1 describes a line-of-sight (LOS) scenario with a separation distance between the transmitter and receiver of less than 4 m. CM2 describes the same range but for a non-LOS situation. CM3 describes a non-

LOS scenario for distances of 4 to 10 m between a transmitter and a receiver. CM4 describes an environment with strong delay dispersion, resulting in a delay spread of around 25 ns. Table 2.1 provides the model parameters of CM1 to CM4.

The time domain expression for the channel impulse response is defined by

$$h(t) = X\sum_{i=0}^{L-1}\sum_{m=0}^{M-1}\alpha_{mi}\delta(t - T_i - \tau_{mi}) \tag{2.19}$$

Where:

$h(t)$ is the channel impulse response

L is the number of clusters

M is the number of rays of each cluster

α_{mi} is the fading coefficient of the m^{th} path of the i^{th} cluster

X is the channel fading factor

T_i is the arrival time of the i^{th} cluster

τ_{mi} is the delay of the m^{th} path of the i^{th} cluster relative to T_i

Generally, there are six key model parameters that define this standard channel. These are: cluster arrival rate (Λ), ray arrival rate (λ), cluster decay factor (Γ), ray decay factor (γ), standard deviation of cluster lognormal fading term (σ_1), standard deviation of ray lognormal fading term (σ_2) and standard deviation of lognormal shadowing term for total multipath realization (σ_x).

The distribution of cluster arrival time and the ray arrival time are given by

$$p((T_i|T_{i-1}) = \Lambda e^{[-\Lambda(T_i - T_{i-1})]}, \qquad i > 0 \tag{2.20}$$

$$p(\left(\tau_{k,i}\middle|\tau_{(k-1),i}\right) = \lambda e^{\left[-\lambda\left(T_{k,i} - T_{(k-1),i}\right)\right]}, \qquad k > 0 \tag{2.21}$$

Mean excess delay, RMS delay spread, number of multipath components (defined as the number of multipath arrivals that are within 10 dB of the peak multipath arrival) and power decay profile the main characteristics of the channel that are used to derive the above model parameters.

But since it is difficult to match the model parameters with the average power decay profile, the main channel characteristics that are used to determine the model parameters are the first three.

Table 2.1: Multipath channel characteristics and corresponding model parameters [10]

Model Parameters and Characteristics	CM 1	CM 2	CM 3	CM 4
Model Parameters				
Λ (1/nsec)	0.0233	0.4	0.0667	0.0667
λ (1/nsec)	2.5	0.5	2.1	2.1
Γ	7.1	5.5	14.00	24.00
γ	4.3	6.7	7.9	12
σ_1 (dB)	3.3941	3.3941	3.3941	3.3941
σ_2 (dB)	3.3941	3.3941	3.3941	3.3941
σ_x (dB)	3	3	3	3
Model Characteristics				
Mean excess delay, τ_m (nsec)	4.9	9.4	13.8	26.8
RMS delay, τ_{rms} (nsec)	5	8	14	26
NP_{10dB}	13.3	18.2	25.3	41.4
NP (85%)	21.4	37.2	62.7	122.8
Channel energy mean (dB)	-0.5	0.1	0.2	0.1
Channel energy std (dB)	2.9	3.3	3.4	3.2

A complex tap model was not adopted here. The complex baseband model is a natural fit for narrowband systems to capture channel behavior independently of carrier frequency, but this motivation breaks down for UWB systems where a real-valued simulation at RF may be more natural. In addition, since the log-normal shadowing of the total multipath energy is captured by the term, X, the total energy contained in the terms $\{\alpha_{mi}\}$ is normalized to unity for each realization. This shadowing term is characterized by $20log10(X) \propto Normal(0, {\sigma_x}^2)$.

Figure 2.11 depicts the discrete time channel impulse response for the four channel types of the standard IEEE 802.15.3a channel model. As it can be seen from the plot, CM1 has considerable magnitude response up to 50ns, CM2 up to 75ns, CM3 up to 120ns and CM4 up to 200ns. This is due to the characteristics of the four channel types. CM1 is designed for LOS and CM4 is designed for highly NLOS scenarios.

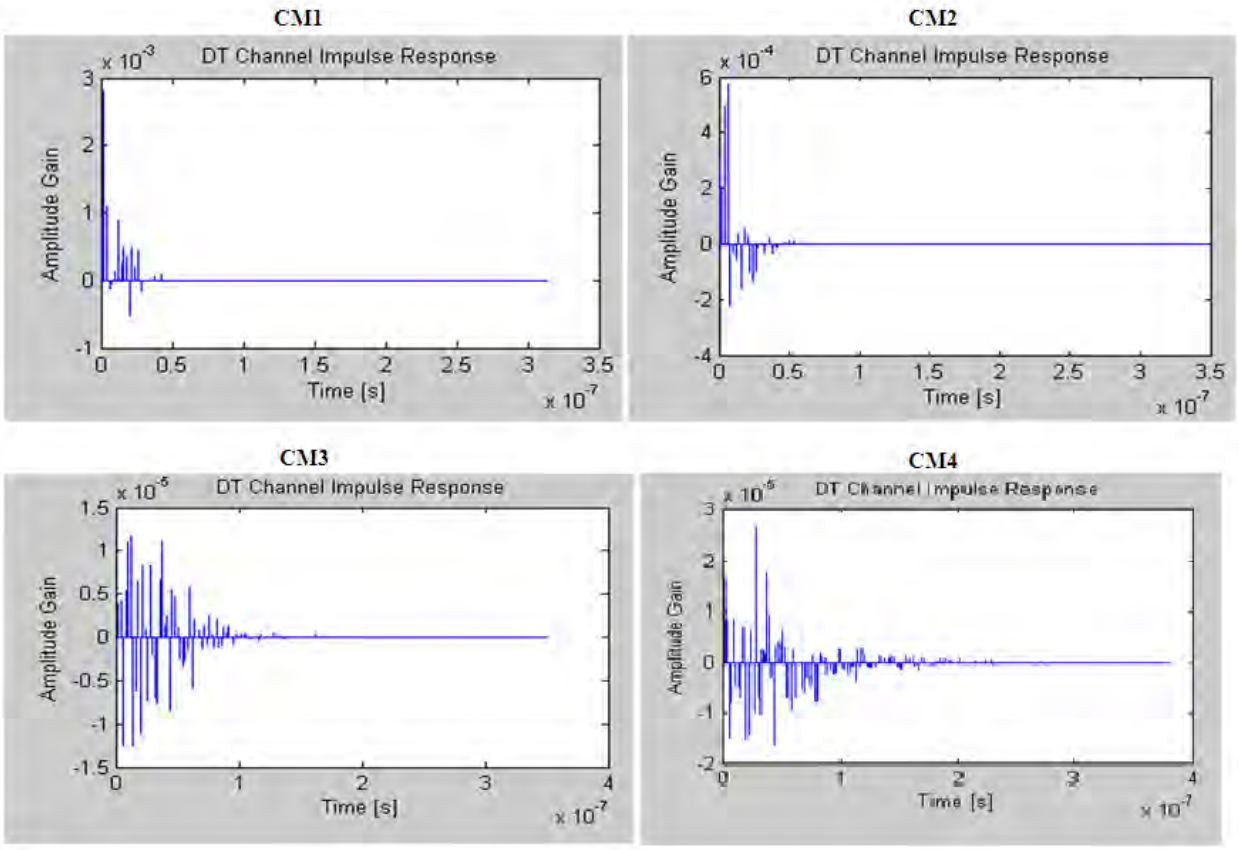

Figure 2.11: Discrete time impulse response for the four channel types of standard model

2.3. Received Signal Model

Consider a multiuser UWB system with K users. The k^{th} user transmits a single-band UWB signal $s_k(t)$ $(k = 1, 2, \dots, K)$ carrying information sequence ${d_j}^k \in [-1, 1]$ as described in Section 2.1.3. The channel impulse response of the k^{th} user for the standard IEEE 802.15.3a channel model discussed in section 2.2.2 can be written as

$$h_k(t) = X_k \sum_{i=0}^{L-1} \sum_{m=0}^{M-1} {\alpha_{mi}}^k \delta(t - {T_i}^k - {\tau_{mi}}^k) \tag{2.22}$$

where the superscript k indicates the user k, ${\alpha_{mi}}^k$ represents the multipath gain coefficients, L denotes the number of resolvable paths, ${\tau_{mi}}^k$ represents the path delays relative to the delay of the desired user's first arrival path, M indicates the number of rays of each cluster and ${T_i}^k$ represents the arrival time of the ith cluster for the desired user.

The signal received consists of multipath signals from all active users and thermal noise. The general expression for the received signal from user *k* can be written as

$$r(t) = s_k(t) * h_k(t) + n(t) \tag{2.23}$$

where $s_k(t)$ is the transmitted signal format by user *k*, $h_k(t)$ the channel impulse response and $n(t)$ is the additive noise, which is modeled as a real additive white Gaussian noise process with zero mean and two-sided power spectral density $N_0/2$.

Using the channel impulse response for user *k* of the standard IEEE 802.15.3a channel model given in (2.19), the received signal can be modeled as

$$r(t) = X_k \sum_{k=1}^{K} \sum_{i=0}^{L-1} \sum_{m=0}^{M-1} {\alpha_{mi}}^k s_k(t - {T_i}^k - {\tau_{mi}}^k) + n(t) \tag{2.24}$$

In order to detect the information in the received signal $r(t)$ different UWB receiver types are proposed in the literature. But in this thesis, detecting the received using RAKE and adaptive MMSE receivers will be discussed in detail. The basic features and performance of RAKE receiver are discussed in chapter 3 and chapter 4 deals adaptive MMSE receiver. Without loss of generality, we let user 1 be the desired user and assume that $\tau^{(1)}(0) = 0$.

Chapter 3

RAKE Receiver for UWB Wireless Communication Systems

3.1. Introduction

Multipath is a common phenomenon that is manifested during the transmission of wireless signals. In this process the transmitted signal proceeds towards its receiver along multiple routes while reflecting, scattering and dispersing due to obstacles it encounters on the way.

The transmitted signal bandwidth in UWB systems is much larger than the coherent bandwidth of the channel, in which case the channel is frequency selective [9]. In frequency selective channels the RAKE principle is conceived as one that employs a certain type of signal processing to different portions of the received signal stream and takes advantage of all the received signal paths that carry the same signal information.

The idea behind the RAKE reception technique is that the signals propagating through different multipath are received in individual fingers of the RAKE receiver, and the outputs from these fingers are then coherently combined to provide the input signal for the symbol decision. An ideal RAKE receiver collects the signal energy from all different multipath components. In practice, however, not all of multipath components can be collected; the N strongest paths must obviously be acquired. The continually acquisition of the multipath components is known as multipath searching and must be done periodically to ensure the N strongest paths are always used for combining.

The optimal RAKE receiver actually implements a channel matched filer which maximizes the received signal to noise ratio. This means that the identified multipath components are weighted proportionally to the amplitude of the component. Of course, the optimal RAKE receiver can only be implemented if the multipath components or the channel impulse response are known.

3.2. RAKE Receiver Structure

A typical RAKE receiver is composed of several correlators followed by a linear combiner, as shown in Figure 3.1. The signal received at the RAKE receiver is correlated with delayed versions of the reference pulse $\{m(t-\tau_i)_{i=0}^{N-1}\}$, multiplied by the tap weights $\{(w_i)_{i=0}^{N-1}\}$, and finally, combined linearly.

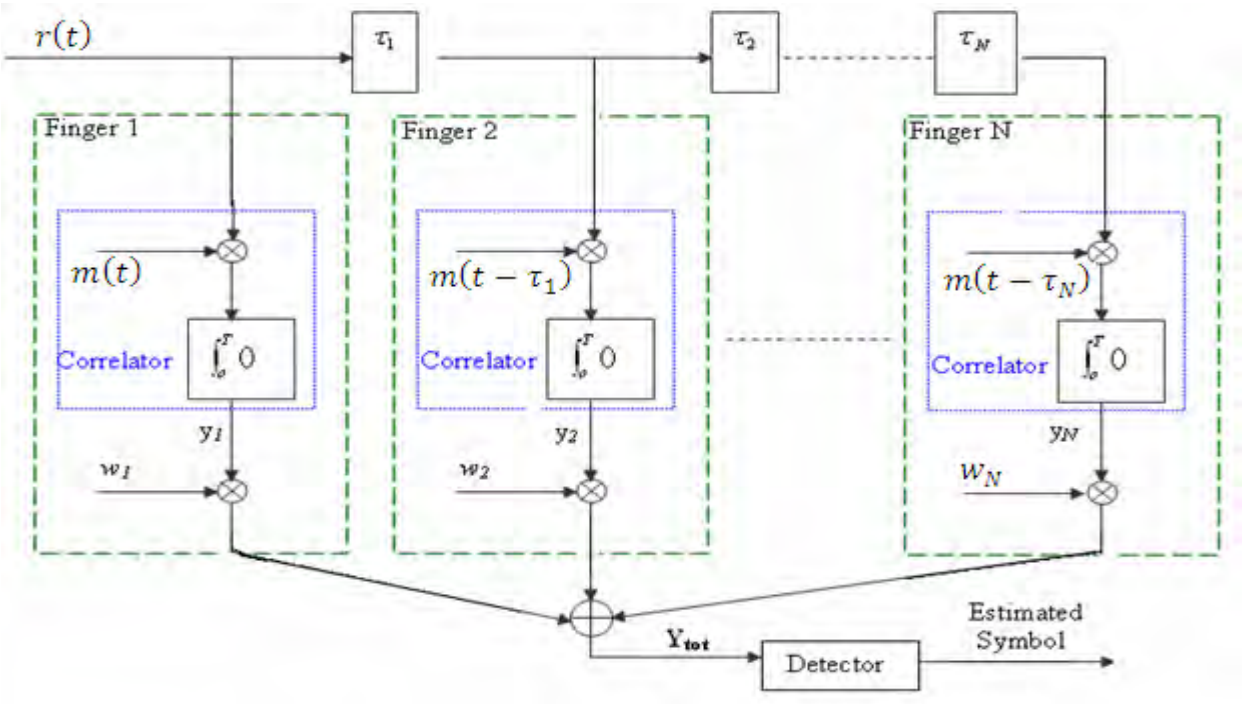

Figure 3.1: Block diagram of RAKE receiver with N fingers

A reference or template signal matched to the incoming received signal is used by the RAKE receiver. Each finger of the RAKE uses a delayed version of the template signal to match the delay to a specific multipath component. This reference signal, also known as the *correlation mask,* depends on modulation and multiple access techniques (transmitted signal format) used at the transmitter.

- The reference signal for TH-PPM-UWB transmitted signal format depends on the PPM delay T_d and is given by

$$m(t) = g_2(t - iT_f - c_iT_c) - g_2(t - iT_f - c_iT_c - T_d) \quad (3.1)$$

- The reference signal used in a TH-BPSK-UWB system is the delayed version of the monocycle received and is given by

$$m(t) = g_2(t - iT_f - c_iT_c) \quad (3.2)$$

- The DS-BPSK-UWB reference signal is a sequence of pulses whose polarities are modulated with the desired user's spreading code and is given by

$$m(t) = \frac{1}{\sqrt{N_c}} \sum_{i=0}^{N_c-1} C_i \; g_2(t - iT_f - C_i T_c) \tag{3.3}$$

Depending on the diversity method implemented at the receiver a different set of weighting factors, $\{w_0, w_1, \ldots, w_N\}$, is used to combine the outputs of the correlators. The output of the linear combiner gives the decision variable, Y_{tot}, which in turn is fed to the detector for the decision process on the transmitted symbol.

3.3. Rake Receiver Types

In general, the number of resolvable path components in a realistic dense multipath channel (i.e., an indoor channel) is approximately proportional to the transmission bandwidth BW and the coherence bandwidth, B_c, of the channel and is given by

$$L = \left\lfloor \frac{BW}{B_c} \right\rfloor + 1 \tag{3.4}$$

Since BW is very high for a UWB system compared to B_c, the total number of resolvable multipath components L, is very large and it is practically difficult design a RAKE receiver that combines all these multipath components which in turn degrades the performance of the receiver. Complexity and performance issues have motivated studies of reduced-complexity RAKE receivers that process only a subset of the resolved multipath components available. Depending on the number of resolvable multipath components used, RAKE receivers can be further classified into all RAKE (ARAKE), selective RAKE (SRAKE) and partial RAKE receiver (PRAKE) receivers. The three RAKE receiver types are described briefly in [9].

3.3.1. All RAKE Receiver

The term All RAKE has been largely used in the literature to indicate the receiver with unlimited resources (taps or correlators) and instant adaptability, so that it can, in principle, combine *all* of the resolved multipath components [9]. From the energy capture perspective, these types of receivers are very efficient and captures most of the energy carried by a very large number of different multipath signals [32]. Since the number of resolvable multipath components increases with the signal bandwidth as given in (3.4), the number of correlators required for the ARAKE receiver may be quite large for UWB communication systems. However, the number of multipath

components that can be utilized in a typical RAKE combiner is limited by power consumption, design complexity and channel estimation. Thus, we consider the ARAKE receiver only as a benchmark that provides an *upper limit* of achievable performance [9].

3.3.2. Selective RAKE Receiver

The selective RAKE (SRAKE) receiver selects the L_b best paths from a subset of the L available resolved multipath components. To select L_b best paths properly requires keeping track of all L path components, using algorithms to sort all these L paths by the magnitude of their instantaneous path gains, which would require instantaneous and highly accurate channel estimation.

3.3.3. Partial Rake Receiver

The partial RAKE (PRAKE) receiver selects the first nonzero L_p arriving paths, which are not necessarily the best. The partial selection requires neither path amplitude knowledge nor the selection mechanism. It only needs to find the position of the first arriving path [9]. This alleviates the need to sort the multipath components by the magnitude of their instantaneous path gains, which would require instantaneous and highly accurate channel estimation. Thus, PRAKE receiver has less complexity than ARAKE and SRAKE receivers but at the cost of lower performance. It has been shown [9] that the performance loss of PRAKE receiver compared to SRAKE receiver is quite small in a Nakagami fading channel but larger in a Rayleigh fading channel.

3.4. Rake Receiver Combining Techniques

For the combination of different shifted, delayed and attenuated received signals at the RAKE's fingers and for the determination of the desired signal, different combining techniques are used. Maximal ratio combining (MRC), equal gain combining (EGC) and selective combining (SC) are the three most commonly used RAKE receiver combining techniques in CDMA and UWB communication systems.

3.4.1. Maximal Ratio Combining

In this technique, all branches of the RAKE receiver are used simultaneously. The weights in each branch are chosen so that the output SNR is maximized. This is an analytical technique that

works only if the individual signals must have the same phase shift before combining which would require estimation of channel parameters which can be difficult in a fast fading environment or a system that is non-coherent. The RAKE receiver using MRC maximizes the system's instantaneous signal-to-noise ratio (SNR) when no narrowband interference exists. Its performance degrades in the presence of narrowband interference [50].

Assuming that co-phasing has been achieved, the envelope of the resulting combined signal Y_{tot} can be written as

$$Y_{tot} = \sum_{i=0}^{N=1} w_i y_i \tag{3.5}$$

where w_i is the gain factor of each branch and y_i is the output of each finger

The MRC has the advantage of producing an output with an acceptable SNR even when none of the individual signals are themselves acceptable. This technique gives the best statistical reduction of fading of any known linear diversity combiner. The drawback with maximal ratio combing is that the receiver tends to be complex, because of the need of measuring the instantaneous SNR in each branch.

Assume that the noise components in the branches are independent. Consequently, the total noise power is given by the sum of the noise power in each branch, where each noise component is multiplied with the combining gain factor of the branch, i.e.

$$N_t = N_0 \sum_{i=0}^{N-1} {w_i}^2 \tag{3.6}$$

Assume that the noise power is equal in all branches. By using the Schwarz inequality, the resulting SNR is

$$SNR = \frac{y^2 E_b}{N_t} = \frac{E_b (\sum w_i y_i)^2}{N_0 \sum {w_i}^2} \leq \frac{E_b}{N_0} \frac{\sum {w_i}^2 \sum {y_i}^2}{\sum {w_i}^2} = \frac{E_b}{N_0} \sum {y_i}^2 \tag{3.7}$$

In MRC, the outputs of the correlators are weighted in direct proportion to the received signal strength.

$$w_i = k y_i \tag{3.8}$$

where k is an arbitrary constant.

3.4.2. Equal Gain Combining

MRC is the method that maximizes the SNR of the resulting combined signal using variable weighting coefficients. However, the variable weighting capability for the MRC is not convenient since the receiver tends to be complex, because of the need of measuring the instantaneous SNR in each branch. A natural step to decrease the complexity is the Equal Gain Combing (EGC) method. In this technique, outputs of the correlators are summed together directly and fed to the detector and it is relatively the simplest form of combiner that does not require any knowledge of the path amplitudes. The weights in this scheme are chosen to remain constant and equal in all branches:

$$w_1 = w_2 = \cdots = w_2 \tag{9.9}$$

The resulting total combined output signal from the linear combiner can be written

$$Y_{tot} = \sum_{i=0}^{N-1} y_i \tag{3.10}$$

Under the assumption of equal noise power in all branches, the resulting SNR becomes

$$SNR = \frac{y^2 E_b}{N N_0} = \frac{E_b}{N N_0}\left(\sum_{i=0}^{N-1} y_i\right)^2 \tag{3.11}$$

where N represents the number of RAKE fingers and N_0 the noise power spectral density.

The benefit of using this type of combining is that it allows the receiver to exploit the signals that are received simultaneously on each branch. This dictates that the possibility of producing an acceptable signal from a number of unacceptable input signals is still retained and the performance is marginally inferior to maximal ratio combining.

3.4.3. Selective Combining

This is the simplest RAKE receiver combining technique. In this technique, the receiver simply chooses the signal with the highest SNR of all the signals from the different fingers, and only uses this signal for detection. This RAKE receiver combining technique has the least complexity and poorest performance when compared with maximum ratio combining (MRC) and equal gain combining (EGC) techniques.

The total combined output signal for this combining technique can be expressed as

$$w_i = \begin{cases} 1, if\ |y_i| = \max\{|y_1|, |y_2|, ..., |y_M|\} \\ 0, otherwise \end{cases} \quad (3.12)$$

3.5. Rake Receiver Performance Analysis

The output of the i[th] finger of the RAKE receiver for the k[th] symbol is given by

$$y_{ik} = \int_0^T r(t)m(t-\tau_i)dt \quad (3.13)$$

Assuming a perfect match of the received signal with the reference signal, zero inter-frame and inter-symbol interference, and symbol rate sampling at the output of RAKE fingers, then (3.13) can be rewritten in discrete time as

$$y_{ik} = b_k\sqrt{E_b}\alpha_i + n_{ik} \quad (3.14)$$

where $i = 0, 1, 2, \ldots, L-1$ is the number of fingers and *k* represents the symbol index.

The noise at the output of the correlators which is approximately distributed as $n \sim N(0, {\sigma_n}^2)$ is given by

$$n_{ik} = \int_0^T n(t)m(t-\tau_i) \quad (3.15)$$

The outputs of the correlators for the *k*[th] symbol can be written in vector notation as

$$\boldsymbol{y_k} = b_k\sqrt{E_b}\boldsymbol{\alpha} + \boldsymbol{n_k} \quad (3.16)$$

where $\boldsymbol{y_k} = [y_{0,k}, \ldots, y_{L-1,k}]^T$, $\boldsymbol{n_k} = [n_{0,k}, \ldots, n_{L-1,k}]^T$ and $\boldsymbol{\alpha} = [\alpha_0, \ldots, \alpha_{L-1}]^T$

Depending on the combining technique applied, different tap weight coefficients can be used by the RAKE receiver. Let $\boldsymbol{w} = [w_0, w_1, \ldots, w_{L-1}]$ be the RAKE combining weights. If maximal ratio combining (MRC) technique is used, the amplitudes of the received multipath components are estimated and used as weighing vector $\boldsymbol{w}$ in each finger. In case of ARake, the combining weights are chosen as $\boldsymbol{w} = \boldsymbol{\alpha}$, where $\boldsymbol{\alpha} = [\alpha_0, \alpha_1, \ldots, \alpha_{L-1}]$ are the fading coefficients of the channel. If the set of indices of the *N* best fading coefficients with largest amplitude is denoted by *S*, then the combining weights $\boldsymbol{w}$ of an SRAKE are chosen as follows [36]

$$\boldsymbol{w} = \begin{cases} \alpha_i & i \in S \\ 0 & i \notin S \end{cases} \quad (3.17)$$

Similarly, for PRAKE using the first N multipath components, the weights of MRC combining are given by [36]

$$\boldsymbol{w} = \begin{cases} \alpha_i & i = 0, \dots, N-1 \\ 0 & i = N, \dots, L-1 \end{cases} \tag{3.18}$$

where $N \leq L$.

In case of equal gain combining (EGC) scheme, all the tracked multipath components are weighted with their corresponding signs and combined [6]. The output after RAKE combining is sent to the decision device and can be written as

$$y_{tot} = b_k \sqrt{E_b} \sum_{i=0}^{L-1} w_i \, \alpha_i + \, n_k \tag{3.19}$$

To determine the bit error performance (BER) at the output of the RAKE, the output signal-to-noise (*SNR*) needs to be evaluated. From (3.19), the approximate signal energy and the noise variance at the output of RAKE are evaluated as

$$E(signal^2) = E_b \left(\sum_{i=0}^{L-1} w_i \alpha_i \right)^2 \tag{3.20}$$

$$E(noise^2) = {\sigma_n}^2 \sum_{i=0}^{L-1} {w_i}^2 \tag{3.21}$$

In case of BPSK modulation, for a given SNR per bit γ_b, the approximate expression of BER performance conditioned on a particular channel realization is given by [3]

$$P_e|\alpha(\gamma_b) = Q\left(\sqrt{SNR}\right) \approx Q\left(\frac{\sqrt{E_b (\sum_{i=0}^{L-1} w_i \alpha_i)^2}}{\sqrt{{\sigma_n}^2 \sum_{i=0}^{L-1} {w_i}^2}} \right) \tag{3.22}$$

Similarly, BER performance expressions for PAM and PPM modulations can be derived by following the same steps.

Chapter 4

Adaptive MMSE Receiver for UWB Wireless Communication Systems

4.1. Introduction

Adaptive MMSE receiver is mainly designed for Multiuser Detection (MUD) in the case of multiple users. MUD is the intelligent estimation/demodulation of transmitted bits in the presence of Multiple Access Interference (MAI). MAI occurs in multi-access communication systems (CDMA/ TDMA/FDMA) where simultaneously occurring digital streams of information interfere with each other. An adaptive MMSE receiver is capable of combining energy from the dense multipath environment of UWB systems [38].

RAKE receiver complexity goes up linearly for each path whose energy is exploited. The MMSE complexity is constant and always exploits all multipath energy present that falls in its observation window and is resolvable [38].

While traditional matched filter and RAKE receivers can reject narrowband interference by exploiting the processing gain of the spread spectrum system, the adaptive MMSE receiver offers much greater interference rejection [42, 46].

Figure 4.1 depicts the general block diagram of a typical DS-BPSK-UWB wireless communication system using adaptive MMSE receiver for received signal detection.

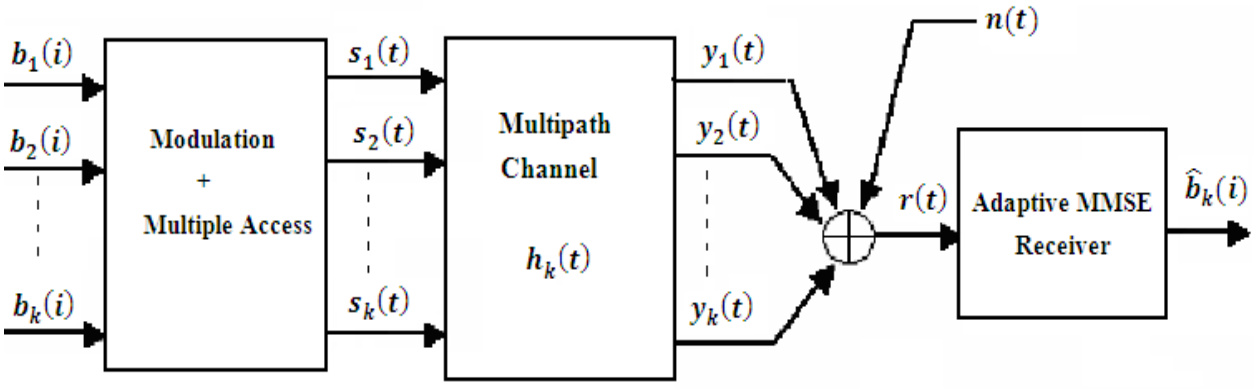

Figure 4.1: Basic block diagram of DS-BPSK-UWB system using adaptive MMSE receiver

4.2. Adaptive MMSE Receiver Structure

The adaptive MMSE receiver consists of a sampling filter and an adaptive filter. The sampling filter samples the total received signal $r(t)$ at least as fast as the Nyquist rate and its output is taken as the adaptive filter's input. The adaptive filter is a finite-impulse response (FIR) filter that essentially acts as a linear corrector with MMSE criterion that minimizes the mean square error (MSE) with different adaptive algorithms.

During each bit decision period, a bit decision $\tilde{b}_k$ is made at the output of the adaptive filter and is then fed back to the adaptive filter to compute MSE. In order to capture enough multipath energy, the observation window of the adaptive filter is typically longer than one bit interval and therefore, windows overlap in time. The whole adaptation works in two stages: *training* and *decision directed* stages. In the training stage, a training sequence is transmitted to adapt the channel. In the decision directed stage, hard decisions are made for information bits and at the same time the tap coefficients are updated with MMSE criterion. Figure 4.2 depicts the general structure of a typical adaptive MMSE receiver for a total of K asynchronous users. LMS, NLMS and RLS adaptive algorithms are used to update the receiver weighting coefficients.

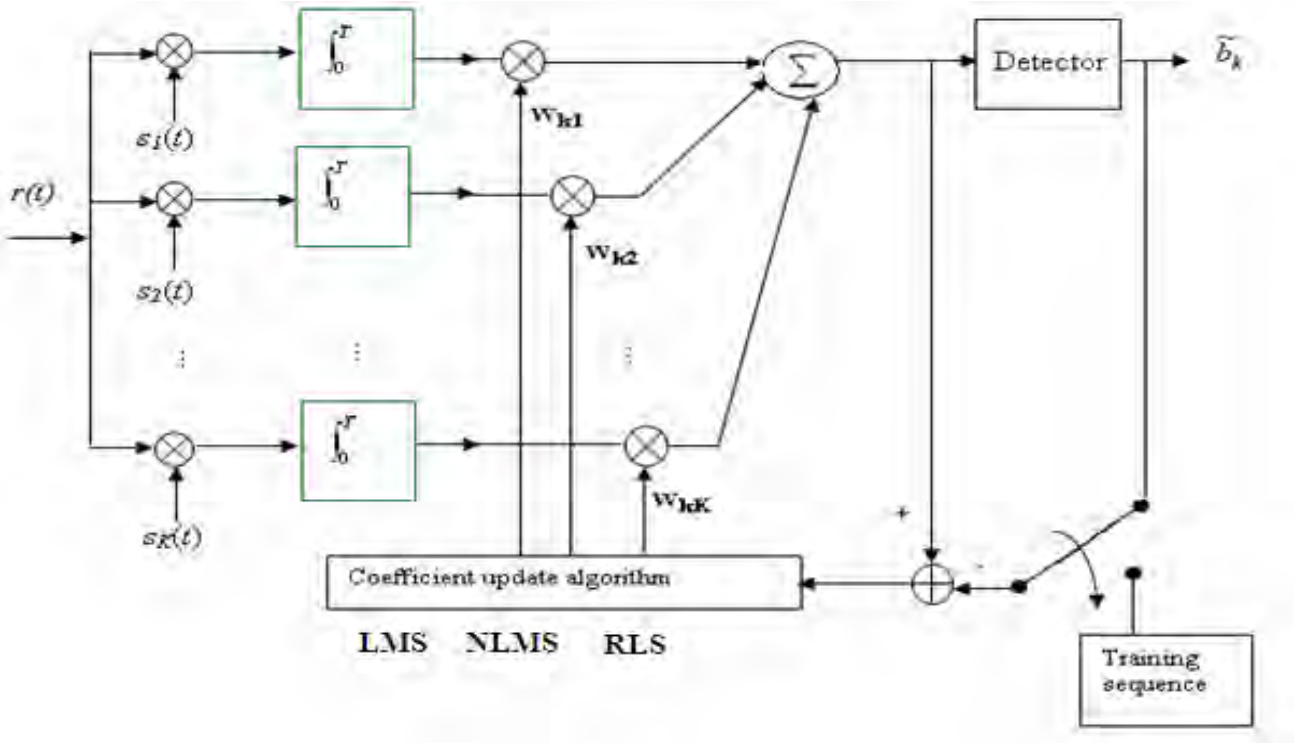

Figure 4.2: General structure of adaptive MMSE receiver

4.3. Adaptive Algorithms

The length M weighting vector $w_k(n)$ contains the coefficients of the transversal filter. The a posteriori error $e_k(n)$ between the transmitted bit $b_k(n)$ and the filter output is given by:

$$e_k(n) = b_k(n) - w_k^T(n)r(n) \tag{4.1}$$

In order to minimize the mean-square error, a weighting vector $w_k(n)$ must be found that minimizes the cost function

$$J(n) = E[(e_k(n))^2] = E[(b_k(n) - w_k^T(n)r(n))^2] \tag{4.2}$$

From (4.2), we can see that the cost function, $J(n)$, is quadratic in $w_k(n)$ and no local minima exist.

The three most commonly used non-blind adaptive algorithms to minimize the cost function, $J(n)$, are the Least Mean Square (LMS), Normalized Least Mean Square (NLMS) and Recursive Least Square (RLS) algorithms [14, 21].

4.3.1. The Least Mean Square (LMS) Algorithm

The LMS algorithm is by far the most widely used adaptive algorithm for several reasons. The main features that attracted the use of the LMS algorithm are low computational complexity, proof of convergence in stationary environment, unbiased convergence in the mean to the Wiener solution, and stable behavior when implemented with finite-precision arithmetic. The LMS update of the filter coefficients that minimize the cost function, $J(n)$ is given by [21]

$$w_k(n+1) = w_k(n) + 2\mu e_k(n)r(n) \tag{4.3}$$

where the convergence factor μ should be chosen in a range to guarantee convergence

4.3.2. The Normalized Least Mean Square (NLMS) Algorithm

The NLMS algorithm utilizes a variable convergence factor that minimizes the instantaneous error. Such a convergence factor usually reduces the convergence time but increases the misadjustment. This algorithm uses the fact that the global minimum of the mean-square error can be found by moving in the direction of the steepest descent on the cost function as given by the opposite direction of the gradient $\nabla J(n)$ with respect to $w_k(n)$. A recursion for updating the filter coefficients can be written as [21]

$$w_k(n+1) = w_k(n) - \frac{1}{2}\gamma(n)\nabla J(n) \tag{4.4}$$

with $\gamma(n)$ determining the step-size of the update in the n^{th} iteration. The gradient can be found from (4.2) as

$$\nabla J(n) = 2E[\left(w_k(n)^T r(n)\right) - b_k(n)r(n)] = -2E[r(n)e_k(n)] \tag{4.5}$$

By ignoring the expectation from (4.5) the gradient can be approximated by

$$\nabla J(n) \cong \widehat{\nabla} J(n) = -r(n)e_k(n) \tag{4.6}$$

The step size is given by

$$\gamma(n) = \frac{\mu}{a + r(n)^T r(n)} \ , a \ll E[r(n)^T r(n)] \tag{4.7}$$

Where μ is the step-size bound to the interval $0 < \mu < 2$ by stability [14, 21]. The constant a is introduced to reduce the effect of gradient noise when $r(n)^T r(n)$ attains a small value.

Selection of the step-size parameter μ is a trade-off between convergence speed and the residual interference. Generally, a small value of μ is desired to minimize residual interference, but this will cause a very slow convergence, which again will require a lot of training bits. As this is not desired a somewhat larger value of μ should be selected as a trade-off between convergence speed and the level of residual interference that can be tolerated by the system.

4.3.3. RLS Algorithm

In RLS algorithm, the cost function to be minimized is given by [14]

$$J(n) = \sum_{i=1}^{n} \lambda^{n-i} [e_k(n)]^2 \tag{4.8}$$

where λ is the exponential weighting factor or forgetting factor. It is a positive constant close to but less than 1. When λ equals 1, we have the ordinary method of least squares. The inverse of $1 - \lambda$ is, roughly speaking, a measure of the memory of the algorithms. The special case, $\lambda = 1$ corresponds to infinite memory.

Define gradient

$$\psi(n) = \frac{\partial w(n)}{\partial \lambda} \tag{4.9}$$

Differentiating the cost function J(n) with respect to λ yields

$$\nabla_{\lambda}(n) = \frac{\partial J(n)}{\partial \lambda} = -\frac{1}{2} E[\psi^{H}(n-1) r(n) \xi^{*}(n) + r^{H}(n) \psi(n-1) \xi(n)] \quad (4.10)$$

The updated weight vector for time *n* is given by gain vector *G(n) = P(n) r(n)*

$$w(n) = w(n-1) + G(n)\, \zeta^{*}(n) \quad (4.11)$$

Where *G(n)* is gain vector

$$G(n) = \frac{\lambda^{-1} P(n-1) r(n)}{1 + \lambda^{-1} r^{H}(n) P(n-1) r(n)} \quad (4.12)$$

And

$$P(n) = \lambda^{-1} P(n-1) - \lambda^{-1} G(n)\, r^{H}(n)\, P(n-1) \quad (4.13)$$

Let S(n) denote the derivative of the inverse correlation matrix *P(n)* with respect to λ:

$$S(n) = \frac{\partial P(n)}{\partial \lambda} \quad (4.14)$$

Differentiating Eq. (4.13) with respect to λ

$$S(n) = \lambda^{-1}[I - G(n)\, r^{H}(n)]\, S(n-1)\, [I - r(n) G^{H}(n)] + \lambda^{-1} G(n)\, G^{H}(n) - \lambda^{-1} P(n) \quad (4.15)$$

Then substituting (4.8), (4.11), and (4.14) in (4.9) yields

$$\psi(n) = [I - G(n)\, r^{H}(n)]\, \psi(n-1) + S(n)\, r(n)\, \zeta^{*}(n) \quad (4.16)$$

According to equation (4.12), the forgetting factor λ(k) is adaptively computed

$$\lambda(n) = \lambda(n-1) + \alpha\, \mathrm{Re}[\psi^{H}(n-1)\, r(n)\, \zeta^{*}(n)] \quad (4.17)$$

Where α is a small, positive learning – rate parameter.

The applicability of the RLS algorithm requires that we initialize the recursion of (4.13) by choosing a starting value P(0) that assures the non-singularity of the correlation matrix [14]. To meet this requirement we may choose the initial value of P(n) with

$$P(0) = \delta^{-1} I \quad (4.18)$$

Where δ is the small positive constant.

And the initial value of weight vector is set to

$$\mathbf{w}(0) = \mathbf{0} \quad (4.19)$$

where **0** is the N-by-1 null vector.

The initialization procedure incorporating Equation (4.18) and (4.19) is referred to as a soft constrained initialization. The positive δ is that it should be small compared to 0.01 σ^2, where σ^2 is the variance of a data sample r(n). Such a choice is based on practical experience with the RLS algorithm supported by a statistical analysis of the soft constrained initialization of the algorithm [14]. Now we may summarize the *RLS algorithm with adaptive memory as follows:*

Starting with the initial values $\hat{w}(0)$, *P(0), λ(0), S(0), and* $\hat{\psi}(0)$, compute for n>0

$$G(n) = \frac{\lambda^{-1} P(n-1) r(n)}{1 + \lambda^{-1} r^H(n) P(n-1) r(n)}$$

$$\zeta(n) = d(n) - \hat{w}^H(n-1)\, r(n)$$

$$w(n) = \hat{w}(n-1) + G(n)\, \zeta^*(n)$$

$$P(n) = \lambda^{-1} P(n-1) - \lambda^{-1} G(n)\, r^H(n)\, P(n-1)$$

$$\lambda(n) = \lambda(n-1) + \alpha\, Re[\hat{\psi}^H(n-1)\, r(n)\, \zeta^*(n)]] \begin{matrix} \lambda_+ \\ \lambda_- \end{matrix}$$

$$\psi(n) = [I - G(n)\, r^H(n)]\ \hat{\psi}^H(n-1) + S(n)\, r(n)\, \zeta^*(n)$$

$$S(n) = \lambda^{-1}[I - G(n)\, r^H(n)]\, S(n-1)\, [I - r(n) G^H(n)] + \lambda^{-1} G(n)\, G^H(n) - \lambda^{-1} P(n)$$

The convergence behavior of the above three algorithms is illustrated by the learning curve given in Figure 4.3 below. The step size for both LMS and NLMS algorithms is $\mu = 0.003$ and the forgetting factor for the RLS algorithm is taken to be $\lambda = 0.86$. These values are arbitrarily selected within the convergence criteria ranges discussed above. The estimated MSE is plotted for 3000 iterations in dB scale. From the given plot, we can observe that RLS algorithm has the fastest convergence and LMS algorithm the lowest convergence. The fastest convergence behavior of the RLS algorithm is achieved at the cost of highest computational complexity compared to LMS and NLMS adaptive algorithms. The computational complexity of the three algorithms is summarized in table 4.1 given below where L represents the order of the lattice filter.

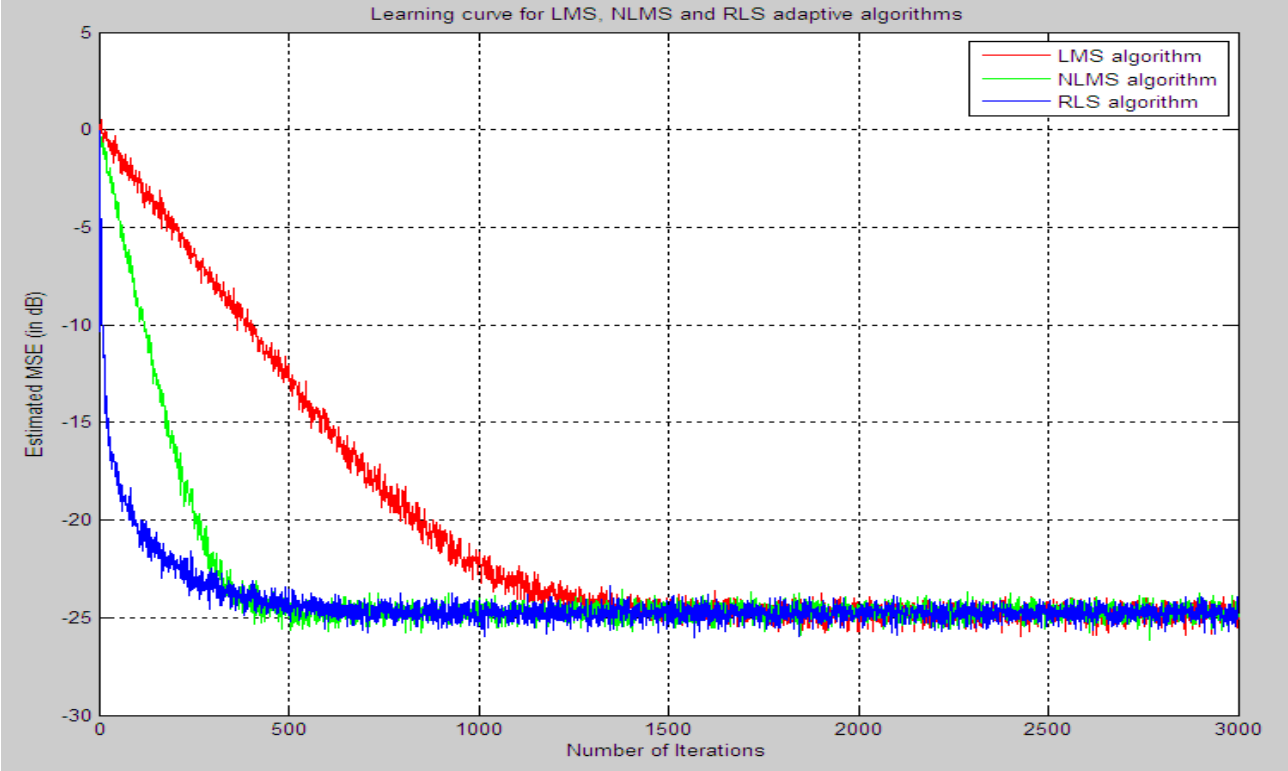

Figure 4.3: Convergence behavior of LMS, NLMS and RLS adaptive algorithms

Table 4.1: Summary of computational complexity of LMS, NLMS and RLS [57]

Adaptive algorithm	Computational Complexity
LMS	2L + 1
NLMS	2L + 3
RLS	18L

4.4. Adaptive MMSE Receiver Performance Analysis

The k^{th} user's signal is transmitted through the multipath channel with impulse response $h_k(t)$. The received signal due to user k is given by

$$y_k(t) = s_k(t) * h_k(t) \tag{4.20}$$

The total received signal due to K users is then given by

$$r(t) = \sum_{k=1}^{K} y_k(t) + n(t) \tag{4.21}$$

where $n(t)$ is zero-mean additive white Gaussian noise (AWGN).

Without loss of generality, we assume that user 1 is the target user. Let the observation window of the adaptive MMSE filter be of duration T_w. The i^{th} window is given by

$$[\, t_0 + (i-1)T_b,\ \ t_0 + (i-1)T_b + T_w] \tag{4.22}$$

Where t_0 is the reference time and $T_b \triangleq 1/symbol\ rate$

For notational simplicity, we employ a discrete time model. The received signal $r(t)$ in (4.21) is first filtered by a bandpass filter to suppress out-of-band noise, assisting convergence of the adaptive filter and then sampled at a rate f_s greater than the Nyquist rate. Define

$$T_s \triangleq \frac{1}{f_s}\ ;\ N_b \triangleq \frac{T_b}{T_s}\ ;\ N_w \triangleq \frac{T_w}{T_s}\ ;\ j_0 \triangleq \frac{t_0}{T_s} \tag{4.23}$$

$$\tilde{y}_k(j) \triangleq y_k(jT_s)\ ;\ \tilde{r}(j) \triangleq r(jT_s)\ \ and\ \tilde{n}_k(j) \triangleq n_k(jT_s)$$

N_w, N_b and j_0 are the sampling numbers of observational window of the adaptive MMSE receiver, the sampling numbers in one symbol and the start point of the observational window respectively and let $Nw > Nb$. We define also two non negative numbers L_1 and L_2 so that $\{\tilde{y}_k(j)\}_{k=1}^{K}$ are all within L_1+L_2+1 observational window. Therefore, we can consider that the k^{th} multi-path signal $\tilde{y}_k(j)$ is divided into L_1+L_2+1 segments. Each segment is length of N_w and is overlapped with N_w -N_b sampling numbers. Parsing the signal $\tilde{y}_k(j)$ into overlapping segments that represent its contribution to each observation window that it affects, we will get

$$v_k(l) = [\tilde{y}_k(j_0 + lN_b + 1), \tilde{y}_k(j_0 + lN_b + 2), \dots, \tilde{y}_k(j_0 + lN_b + N_w)]^{\,T} \tag{4.24}$$

where l=-L_1, -L_1+1, …, L_2 and $\tilde{y}_k(j) = 0$ outside the finite IR of the channel.

The content of each observational segment denotes that user k impacts on user 1 within the segment. Note that the i^{th} bit decision for user 1 occurs in window i.

Denote the adaptive filter taps by **w**, and the received signal in the i^{th} bit's observation window by **u(i)**, as given below:

$$\boldsymbol{w} \triangleq [w(1), w(2), \dots, w(N_w)]^T \tag{4.25}$$

$$\boldsymbol{u}(i) \triangleq [\tilde{r}(j_0 + (i-1)N_b + 1), \tilde{r}(j_0 + (i-1)N_b + 2), \dots, \tilde{r}(j_0 + (i-1)N_b + N_w)]^T \tag{4.26}$$

Substituting (4.21), (4.23) and (4.24) into (4.26), we get

$$u(i) = \sum_{k=1}^{K} \sum_{l=-L_1}^{L_2} b_k\,(i-l) v_k(l) + \; n(i) \tag{4.27}$$

where $n(i) = [\tilde{n}(j_0 + (i-1)N_b + 1), \tilde{n}(j_0 + (i-1)N_b + 2), \ldots, \tilde{n}(j_0 + (i-1)N_b + N_w)]^{\,T}$ is an AWGN noise vector within the observational window.

The optimal MMSE filter taps $\tilde{w}$ to detect user 1's i^{th} bit are given by

$$\begin{aligned} \tilde{w} &= \arg\min_w E\{|b_1(i) - w^H u(i)|^2\} \\ &= \arg\min_w E\{w^H E[u(i)u^H(i)]w - 2Re\{w^H E[b_1(i)u(i)]\}\} \end{aligned} \tag{4.28}$$

Let $E[b_1(i)u(i)] = v_1(0)$, $E[u(i)u^H(i)] = \sum_{k=1}^{K}\sum_{l=-L_1}^{L_2} v_k\,(l){v_k}^H(l) + \; E[n(i)n^H(i)]$ and $R_{nn} = E[n(i)n^H(i)]$. Then for mutual statistically independent $b_k(i)$ and $n(i)$, (4.28) becomes

$$\tilde{w} = \left[\sum_{k=1}^{K} \sum_{l=-L_1}^{L_2} v_k(l){v_k}^H(l) + R_{nn}\right]^{-1} v_1(0) \tag{4.29}$$

Finally, the output of the adaptive MMSE filter becomes

$$\hat{b}(i) = \tilde{w}^H u(i) = \tilde{w}^H v_1(0) b_1(i) + e_{mui}(i) + e_n(i) \tag{4.30}$$

where $e_{mui}(i)$ and $e_n(i)$ denote the residual errors, which are mutual statistically independence Gaussian random variables with zeros mean, variances and respectively), caused by interference users and AWGN noise respectively [37].

Therefore, the close form of the bit error probability of adaptive MMSE receiver can be formulated as [37]

$$P_e = Q\left(\sqrt{\frac{\tilde{w}^H v_1(0)}{{\sigma_{mui}}^2 + {\sigma_n}^2}}\right) \tag{4.31}$$

where ${\sigma_{mui}}^2 = \sum_{k=2}^{K}\sum_{l\neq 0}|\tilde{w}^H v_k(l)|^2$ and ${\sigma_n}^2 = \sigma^2|\tilde{w}|^2$

Chapter 5

Simulation Results and Discussion

5.1. Simulation Setup

In this chapter, simulation results for the BER performance of both RAKE and adaptive MMSE receivers under different situations have been shown. All the simulations are carried out using MATLAB software. Performance analysis and comparison for each result is discussed in detail after different system parameter considerations. The basic simulation functional blocks are given in Figure 5.1 and Table 5.1 provides system parameters that are used in the simulation and their corresponding values. The values for the different simulation parameters are selected in such a way that the whole system meets some standard regulations and have practical applicability.

5.2.1. Simulation Flowchart

Figure 5.1, given below, describes the basic functional blocks that have been used for the simulations and their sequential flow for both RAKE and adaptive MMSE receiver.

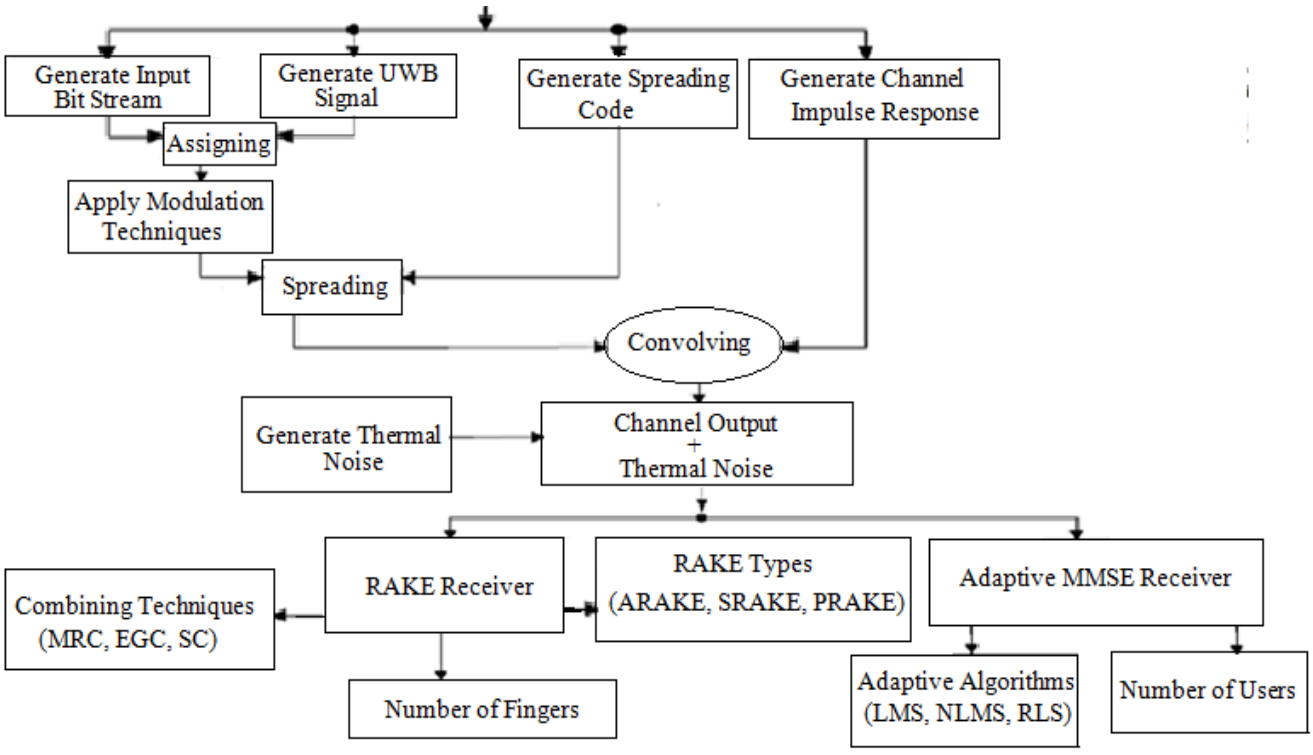

Figure 5.1: General flowchart diagram for basic simulation building blocks

Specifically, the general flowchart for the simulation of the adaptive MMSE receiver is given in Figure 5.2 below.

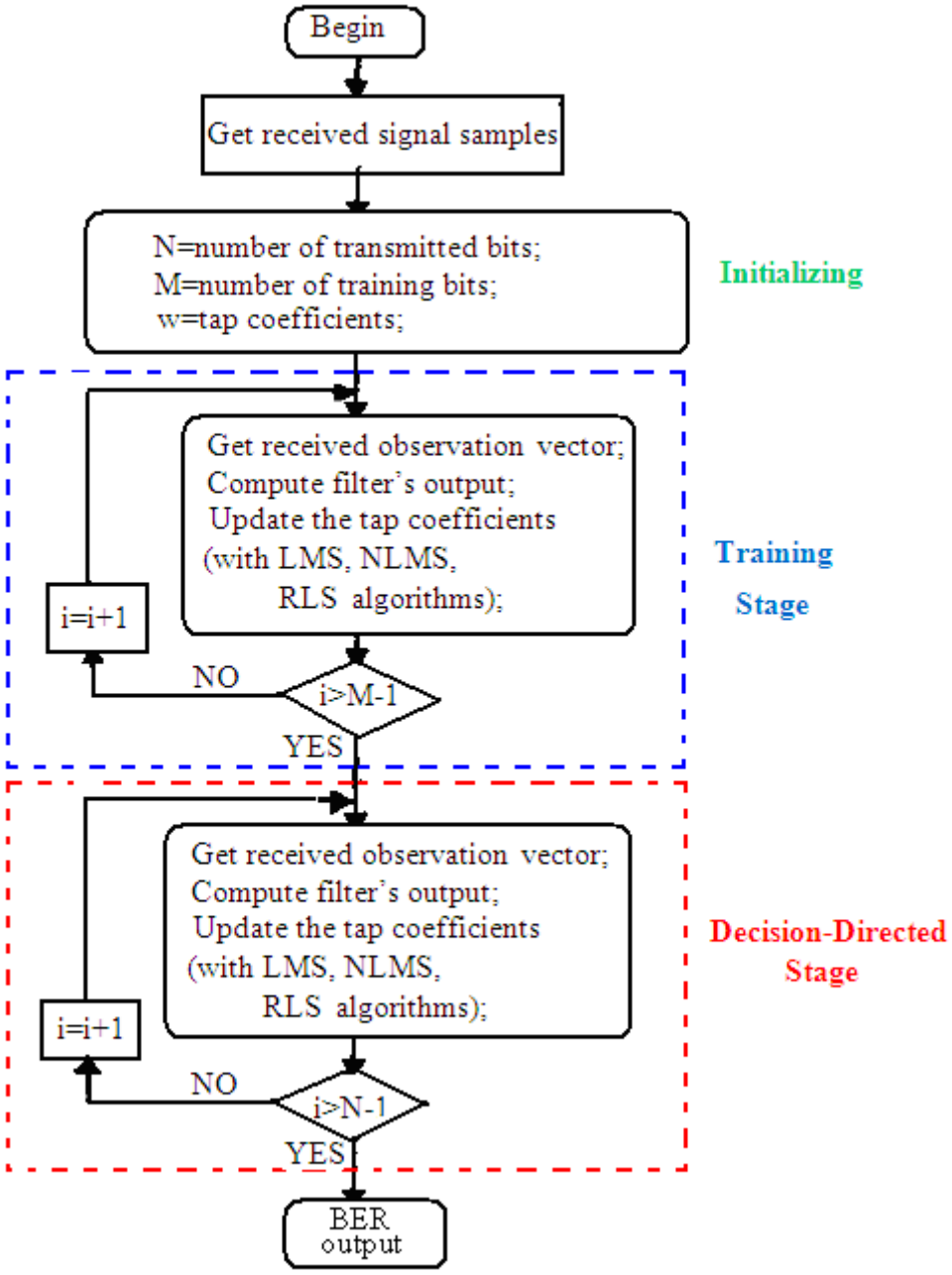

Figure 5.2: Flowchart of the adaptive MMSE receiver detection principle

5.2.2. Simulation Assumptions and Parameters

In this thesis work, a number of assumptions have been made during simulation. Some of these basic assumptions include:

- All users randomly access the channel
- User transmits at equal power level or perfect power control is assumed
- Received signals at the receiver have the same power level
- The receiver has perfect channel knowledge or perfect channel estimation is assumed
- Perfect carrier and time synchronization between the transmitter and receiver is assumed

The various parameters and their values that are used during simulation of results are described in Table 5.1 below.

Table 5.1: Simulation parameters and their corresponding values

Parameters	Symbol	Value (if any)
Pulse repetition period	T_f	60ns
Chip time (Chip length)	T_c	1ns
Average transmitted power	P	-40dBm
Sampling frequency	f_c	50Ghz
Length of transmitted bits	N	10000
Spread gain	N_c	31
PPM delay	δ	0.5ns
Transmitted signal formats	TH-PAM, TH-OOK, TH-PPM, TH-BPSK, DS-BPSK	-
Channel model	Standard IEEE 802.3.15a Channel (CM1,CM2,CM3,CM4)	-
Pulse shape	Second order Gaussian pulse, $[g_2(t)]$	-
Pulse duration (Pulse width)	T_w	0.395ns
Pulse shaping factor	τ	0.2ns
Length of training sequence	M	1000
Adaptive Algorithms	LMS, NLMS, RLS	-
LMS/NLMS convergence factor	μ	0.01
RLS forgetting factor	λ	0.8
Tx-Rx separation distance	d	2m, 4m, 8m
Bit repetition code length	N_s	1, 2, 3, 4

5.2. Performance Evaluation of RAKE Receiver

In this section, the detail BER performance analysis and comparison of RAKE receiver for different system parameters is provided. The performance analysis and comparison includes different RAKE combining techniques, RAKE receiver types, number of RAKE fingers, transmitted signal formats, channel types and bit repetition code lengths.

5.2.1. Performance for Different Combining Techniques

Figure 5.2 compares the BER performance of the three main RAKE receiver combining techniques: MRC, EGC and SC. The simulation is carried out using SRAKE receiver with 10 fingers under CM1. From the given plot, we can see that MRC has the best BER performance at the cost of higher complexity followed by EGC and SC the least BER performance. The complexity depends on the number of resolvable multipath components of the RAKE receiver.

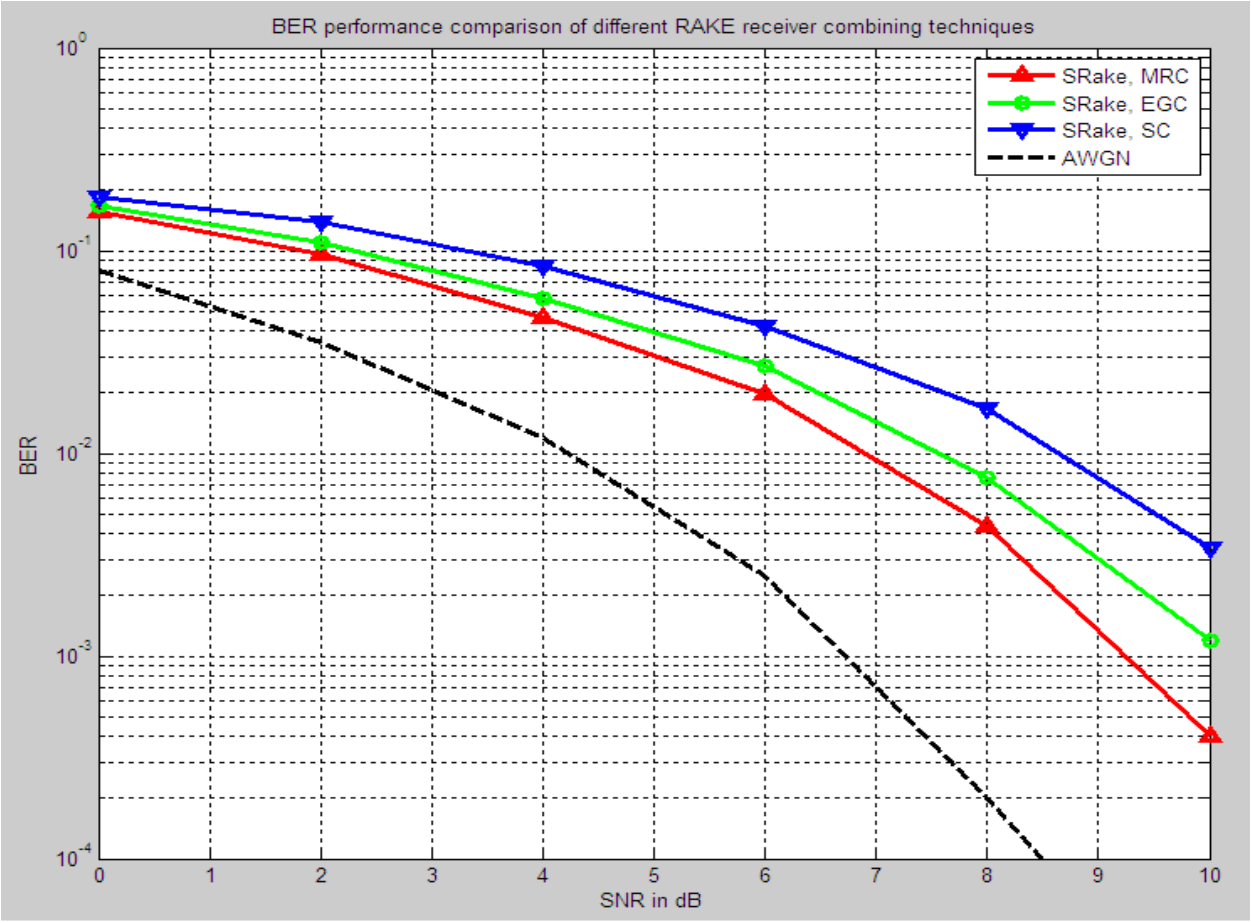

Figure 5.3: BER performance comparison of different RAKE combining techniques

5.2.2. Performance for Different RAKE Types

Figure 5.4 shows the BER performance of ARAKE, SRAKE and PRAKE receivers for TH-PPM-UWB transmitted signal format. In this simulation result, CM3 is considered and MRC is used. SRAKE and PRAKE receivers with 5 and 10 fingers are used for BER performance comparison with the ideal ARAKE receiver.

As anticipated, the ARAKE receiver has the best performance gaining almost 1.2dB SNR over SRAKE receiver with 5 fingers at BER of 0.01. At BER of 0.02, PRAKE receiver with 5 fingers has a SNR loss of about 3dB and PRAKE receiver with 10 fingers has only 1dB SNR loss compared to ARAKE receiver. SRAKE receiver with 10 fingers has nearly the same performance as that of ARAKE receiver. In addition, PRAKE receiver with 10 fingers and SRAKE receiver with 5 fingers have almost the same performance.

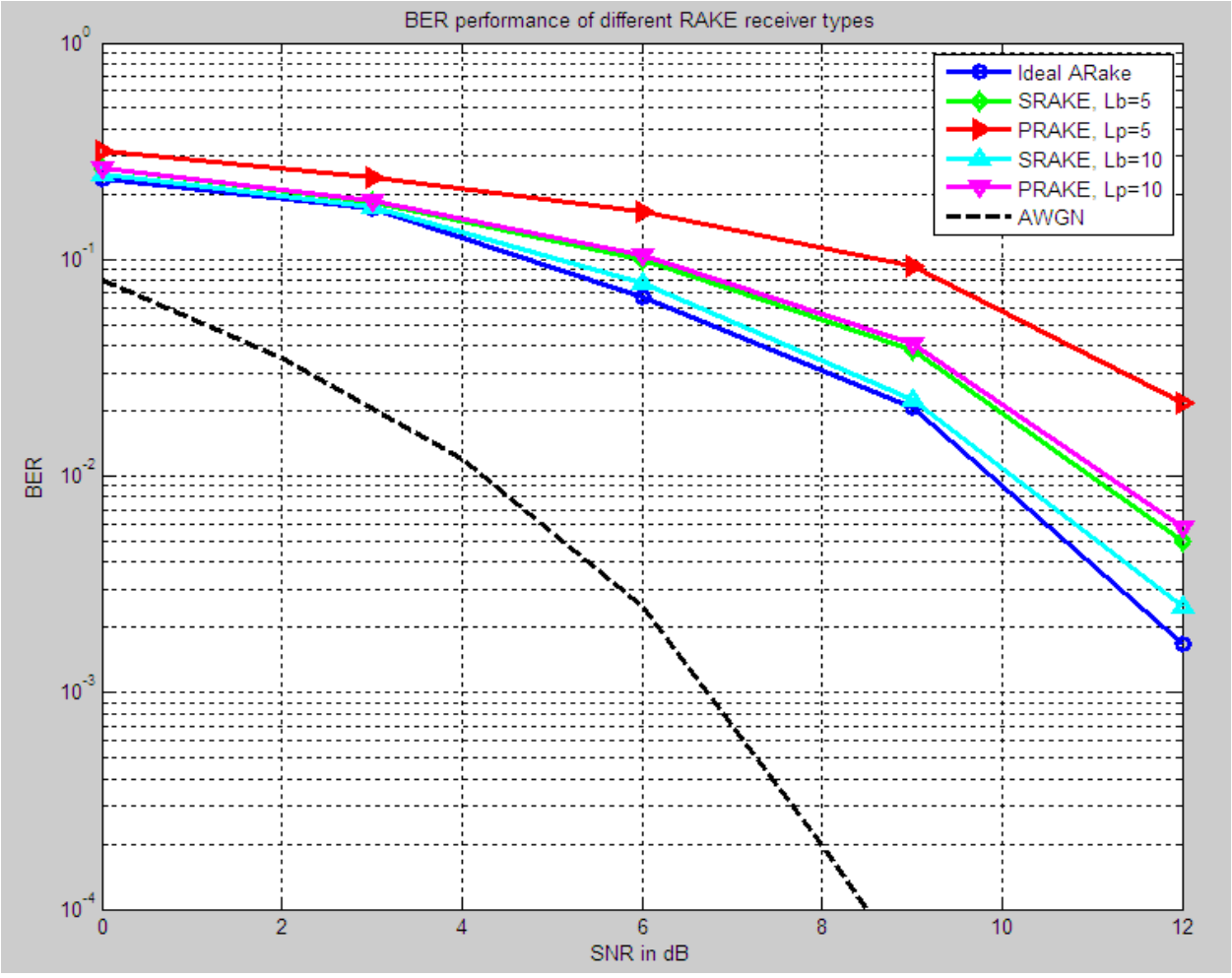

Figure 5.4: BER performance comparison of different RAKE types

5.2.3. Performance for Different Number of RAKE Fingers

BER performance of PRAKE receiver for different number of fingers is compared in Figure 5.5. The simulation result is obtained using TH-PPM-UWB transmitted signal format under CM3. MRC is used for combining the output of the fingers. PRAKE receiver with 2, 5, 10, 15 and 20 fingers is considered for BER performance comparison.

As expected, the BER performance becomes better as we increase the number of fingers. For example, at SNR of 10dB, PRAKE receiver with 2 fingers has BER performance penalty of nearly 0.232 compared to PRAKE receiver with 20 fingers. Actually, this performance improvement is obtained at the cost of increasing the receiver complexity which is nearly 9 times as complex as LMS and NLMS algorithms as shown in Table 4.1. So, in order to make a compromise between complexity and performance RAKE receivers with medium number of fingers are practically used.

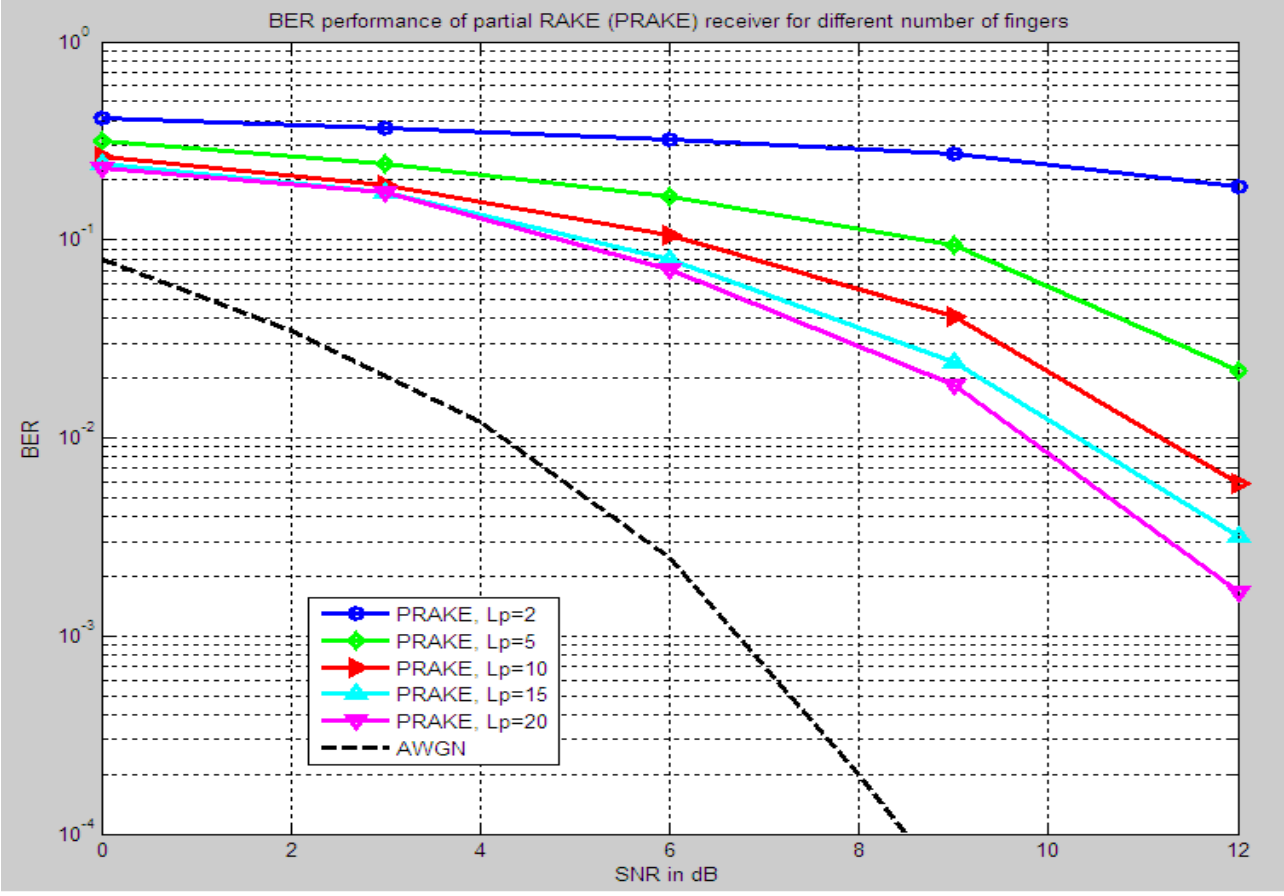

Figure 5.5: BER performance of PRAKE receiver with different number of fingers

5.2.4. Performance for Different Channel Models

Figure 5.6 represents the BER performance of SRAKE receiver with 10 fingers under different channel types (CM1, CM2, CM3 and CM4). The simulation is carried out using TH-BPSK-UWB transmitted signal format and MRC technique.

From the plot, we can see that SRAKE receiver has the best BER performance under CM1 and the worst performance under CM4. This is because CM1 is designed for short distance separation between the transmitter and the receiver and LOS scenario and CM4 for relatively longer separation distance and highly NLOS scenario. At BER of 0.01, CM1 has a SNR gain of around 1.6 dB compared to CM2, 5.6dB compared to CM3 and greater than 6dB compared to CM4.

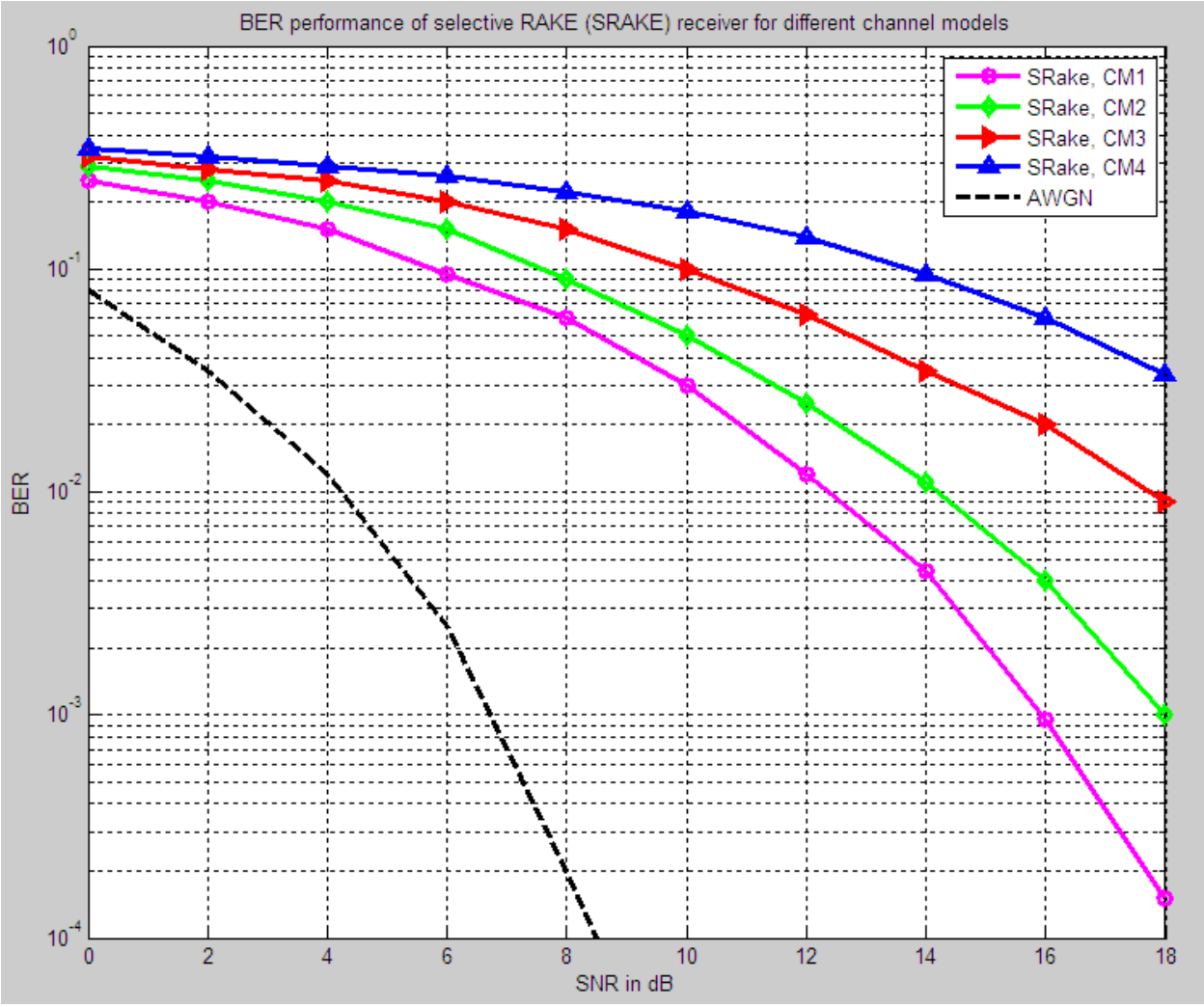

Figure 5.6: BER performance of SRake receiver under different channel types

5.2.5. Performance for Different Transmitted Signal Formats

Figure 5.7 compares the BER performance of SRAKE receiver with 10 fingers for different transmitted signal formats (TH-OOK-UWB, TH-PAM-UWB, TH-PPM-UWB and TH-BPSK-UWB). CM3 is considered and MRC technique is used to get the given simulation result.

The receiver has the poorest performance for TH-OOK-UWB transmitted signal format as OOK modulated signals are highly noise affected and it has the best performance when the transmitted signal format is TH-BPSK-UWB. At SNR of 10dB, SRAKE receiver using TH-BPSK-UWB transmitted signal format has BER performance improvement of around 0.02, 0.03 and 0.11 compared to SRAKE receiver using TH-PPM-UWB, TH-PAM-UWB and TH-OOK-UWB transmitted signal formats respectively.

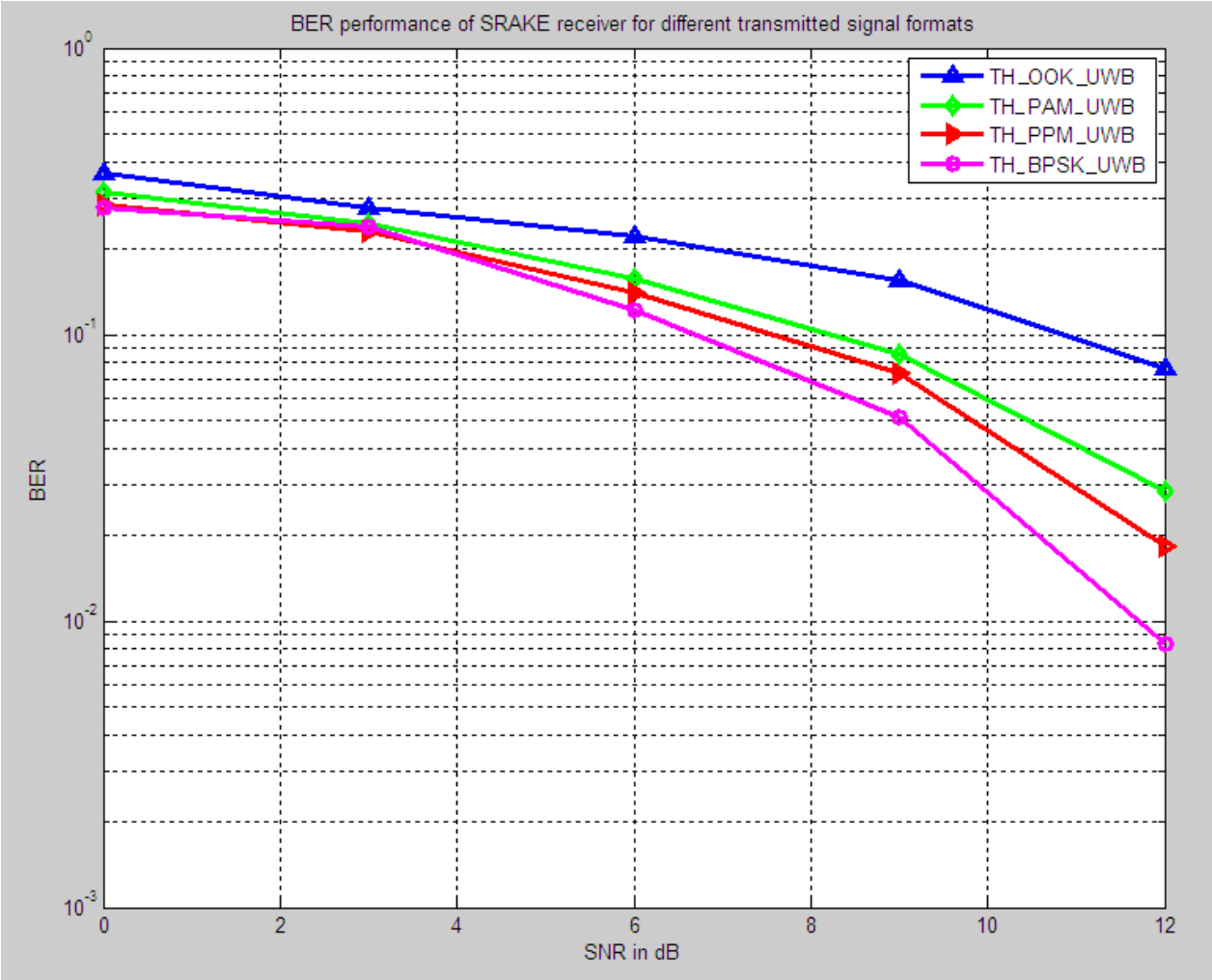

Figure 5.7: BER performance of SRAKE receiver for different transmitted signal formats

5.2.6. Performance for Different Bit Repetition Code Lengths

Figure 5.8 shows the BER performance of SRAKE with 10 fingers for different number of bit repetition code lengths. In this simulation, TH-PPM-UWB transmitted signal format is assumed. In addition, CM1 is considered and MRC technique is used to combine the output of the SRAKE fingers.

As we increase the repetition code length per transmitted data bit, there is a highly significant BER performance improvement of the receiver. At BER of 0.02, the SRAKE receiver with Ns=4 has a SNR gain of around 1.3dB, 2.6dB and 5.6dB compared to the SRAKE receiver with Ns=3, Ns=2 and Ns=1 respectively.

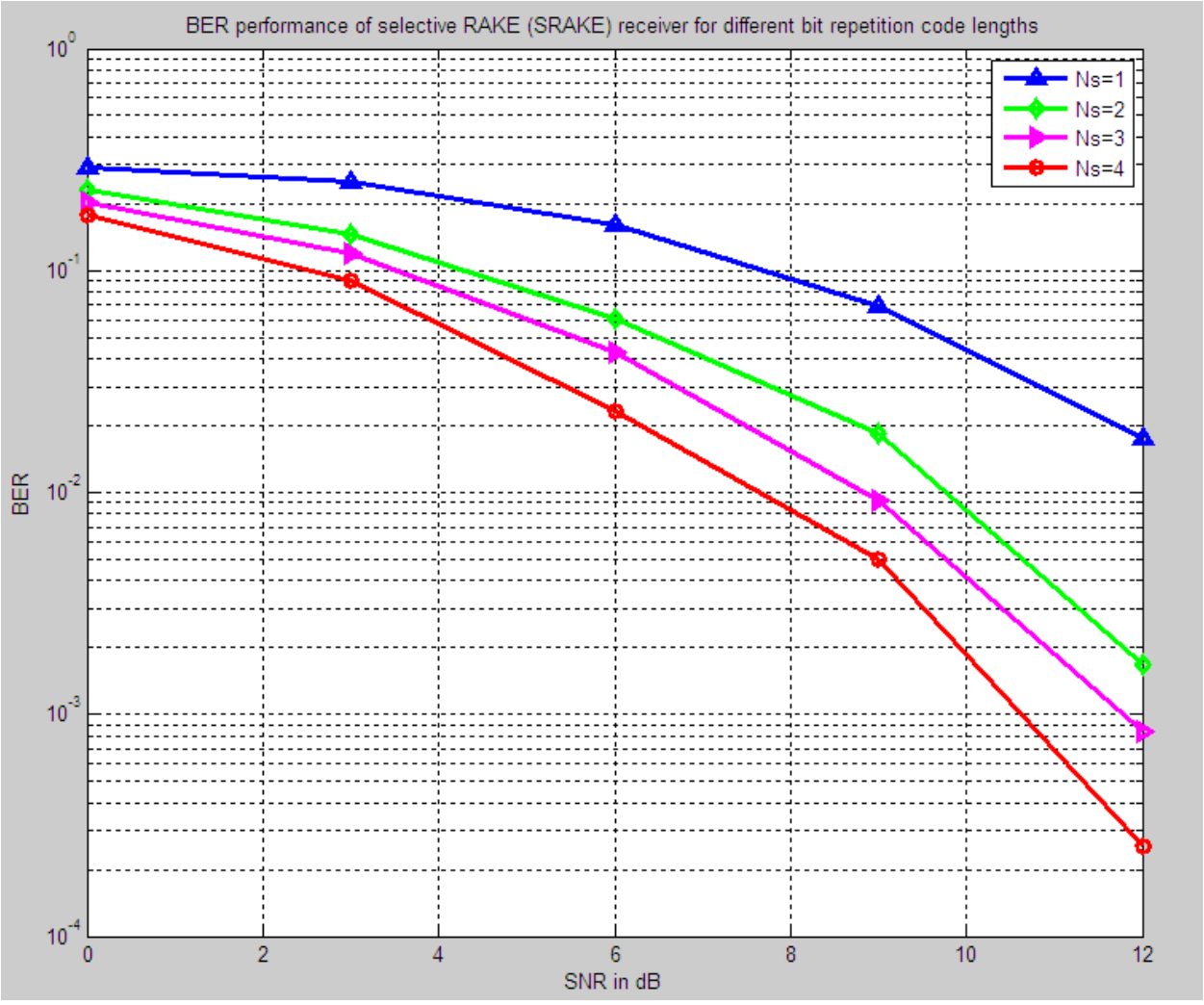

Figure 5.8: BER performance of SRAKE receiver for different bit repetition code lengths

5.3. Performance Evaluation of Adaptive MMSE Receiver

In this section, an extensive BER performance analysis and comparison of adaptive MMSE receiver for adaptive algorithms and number of users is provided.

5.3.1. Performance for Different Number of Users Using LMS Algorithm

Figure 5.9 presents BER performance of adaptive MMSE receiver for different number of asynchronous interfering users using LMS algorithm. We assume that all users transmit the same DS-BPSK-UWB signal format with the same power and CM1 is considered. From the given plot we can see that as the number of interfering users increase the performance degrades rapidly. The receiver has a good BER performance for 5 users, especially at higher SNR and the BER for 30 users is very poor and almost flat for SNR increments.

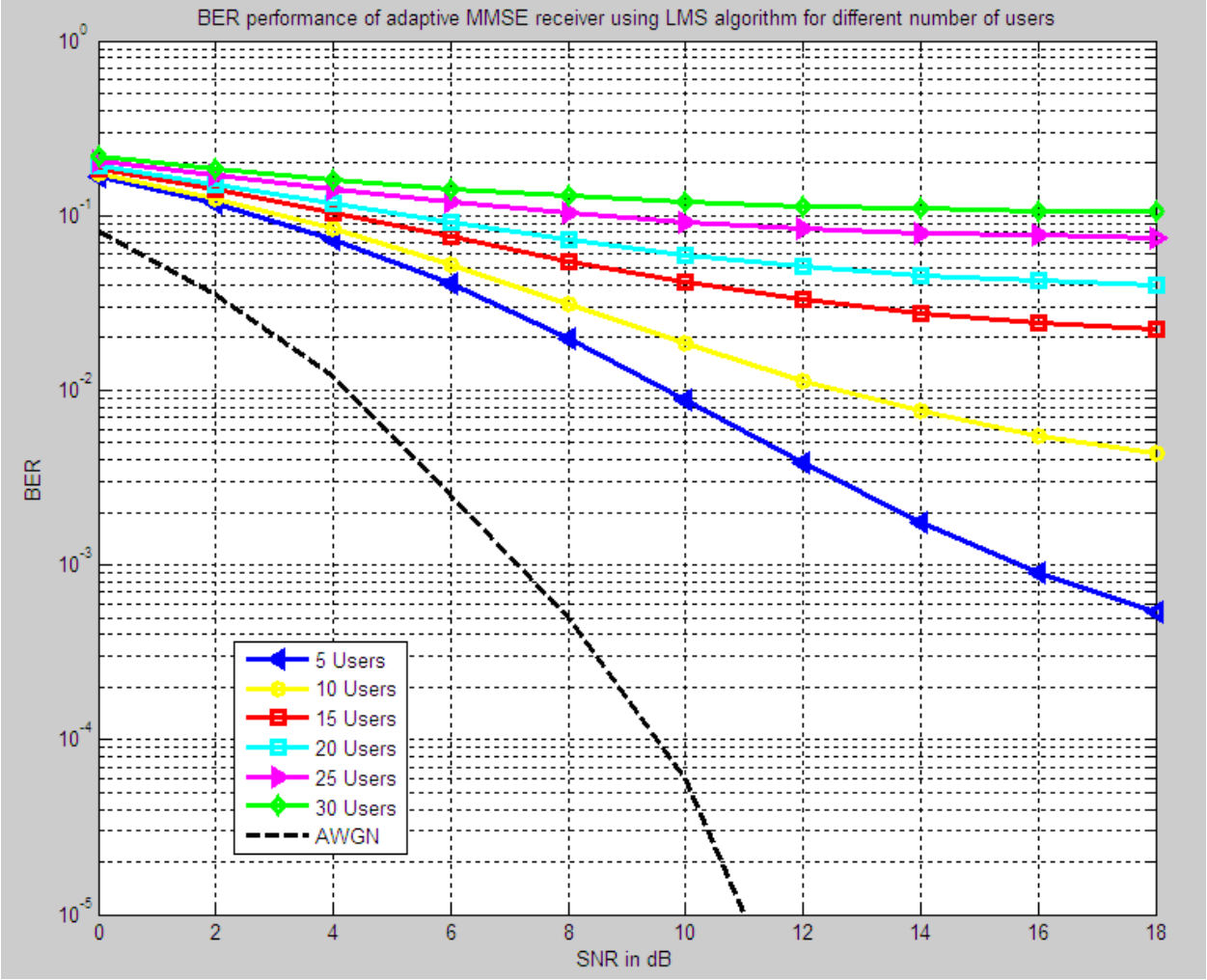

Figure 5.9: BER performance of adaptive MMSE receiver using LMS algorithm

5.3.2. Performance for Different Number of User Using NLMS Algorithm

BER performance of adaptive MMSE receiver for different number of asynchronous interfering users using NLMS algorithm is given in Figure 5.10 below. Here again, we assume perfect power control of all users. The simulation result is obtained for DS-BPSK-UWB signal format and under CM1.

As expected, the BER performance of the receiver decreases as the number of interfering users increase. There is a SNR loss of around 6dB at BER of 0.002 in increasing the number of users from 5 to 10 and this loss becomes even larger for higher number of interfering users.

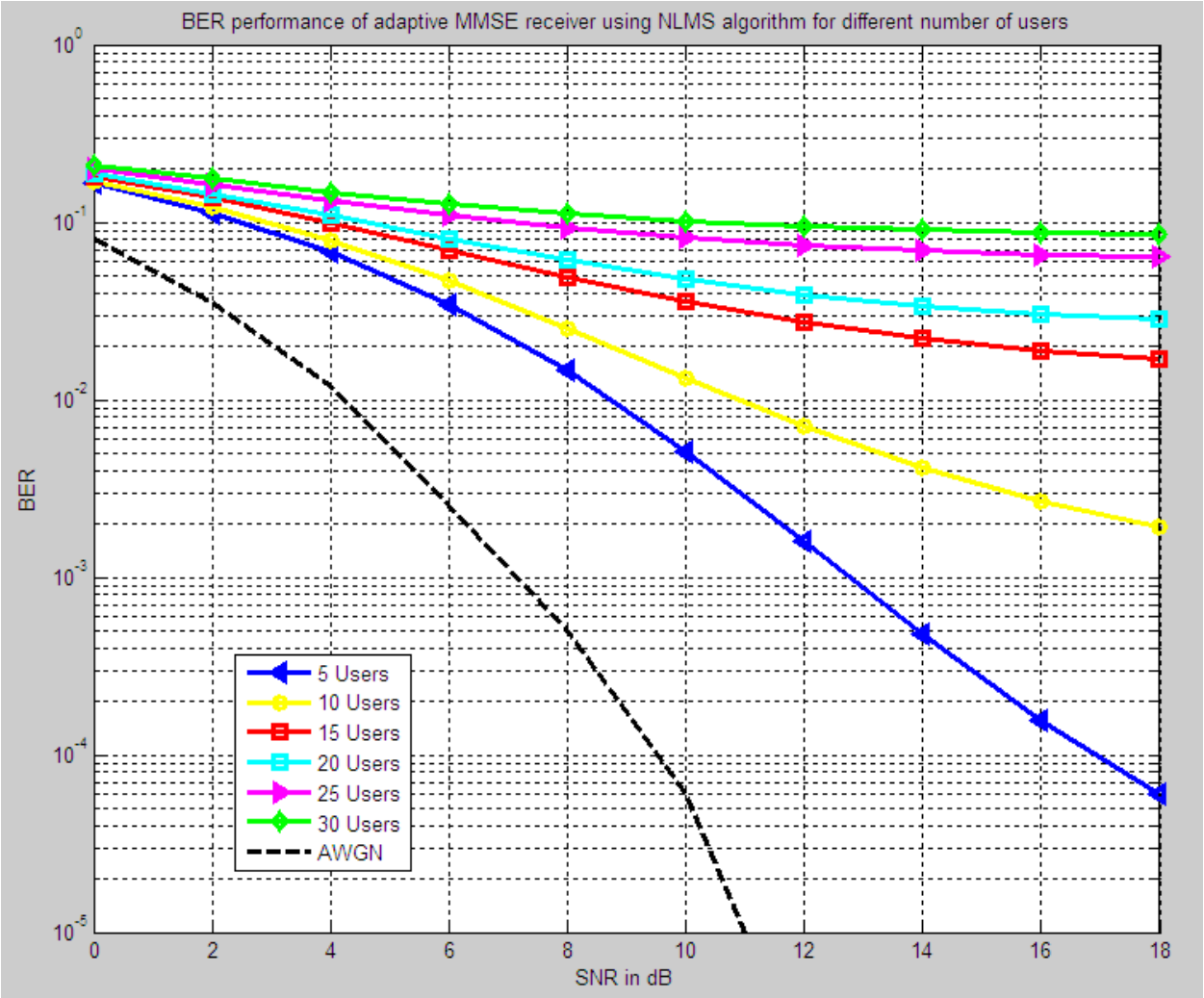

Figure 5.10: BER performance of adaptive MMSE receiver using NMLS algorithm

5.3.3. Performance for Different Number of Users Using RLS Algorithm

Figure 5.11 depicts BER performance of adaptive MMSE receiver for different number of asynchronous interfering users using RLS algorithm. The simulation is carried out, assuming that all users transmit the same DS-BPSK-UWB signal format with the same power and CM1 is considered.

The plot shows the same result as that of LMS and NLMS algorithms. The BER performance of the receiver falls rapidly as we increase the number of interfering users due to MUI effects. But RLS algorithm has better performance even for higher number of users compared to LMS and NLMS algorithms.

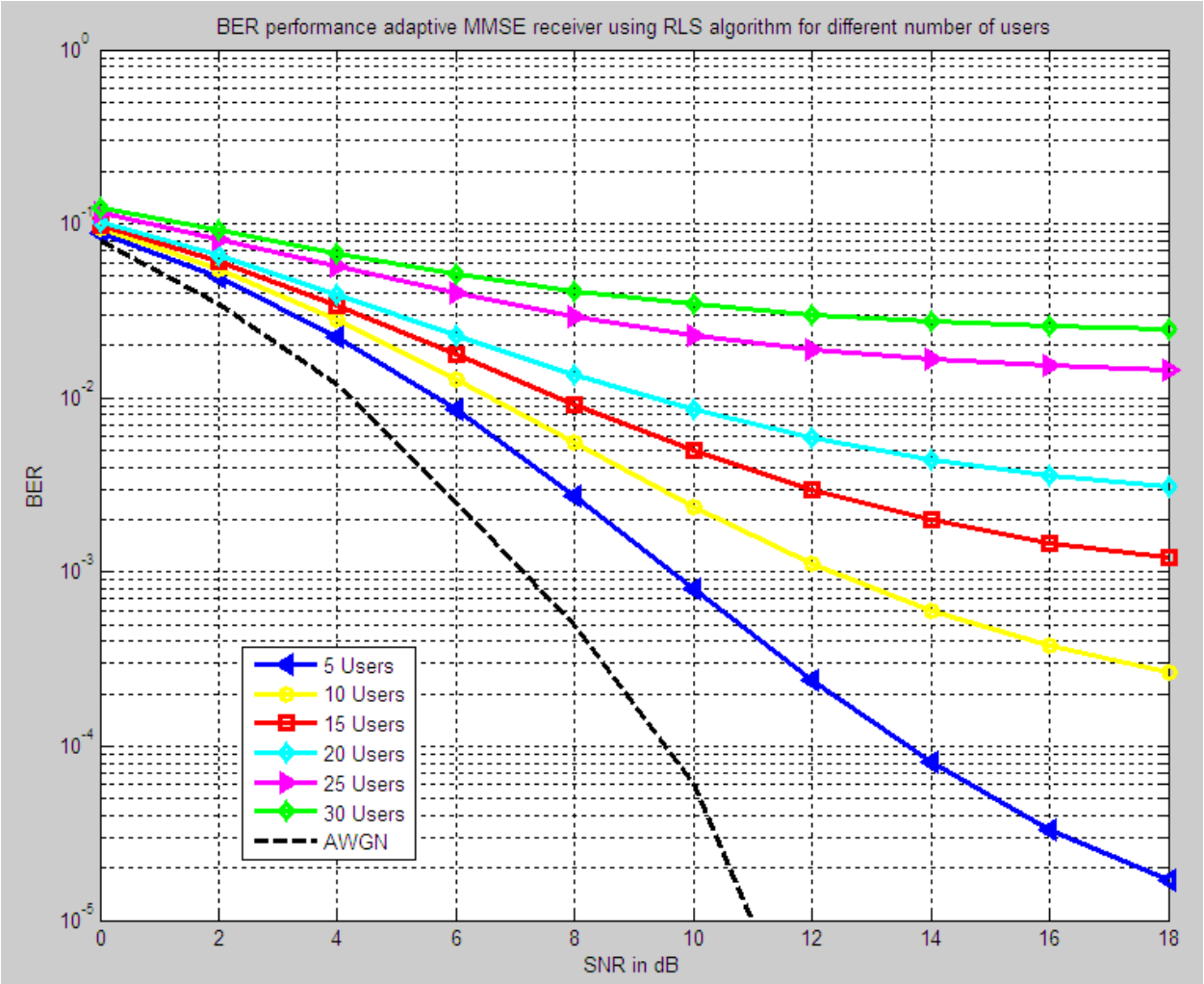

Figure 5.11: BER performance of adaptive MMSE receiver using RLS algorithm

5.3.4. Performance Comparison of Different Adaptive Algorithms

Figure 5.12 compares BER performance of different adaptive algorithms for 5 asynchronous interfering users. In this simulation, perfect power control is assumed for all users. All users transmit the same DS-BPSK-UWB signal format under CM1.

As expected, RLS algorithm has the best BER performance compared to NLMS and LMS algorithms. At SNR of 12 dB, RLS algorithm has a BER performance improvement of around 0.00146 compared to NLMS algorithm and 0.00376 compared to LMS algorithm. But we must not that this performance improvement is obtained at the cost of higher receiver complexity.

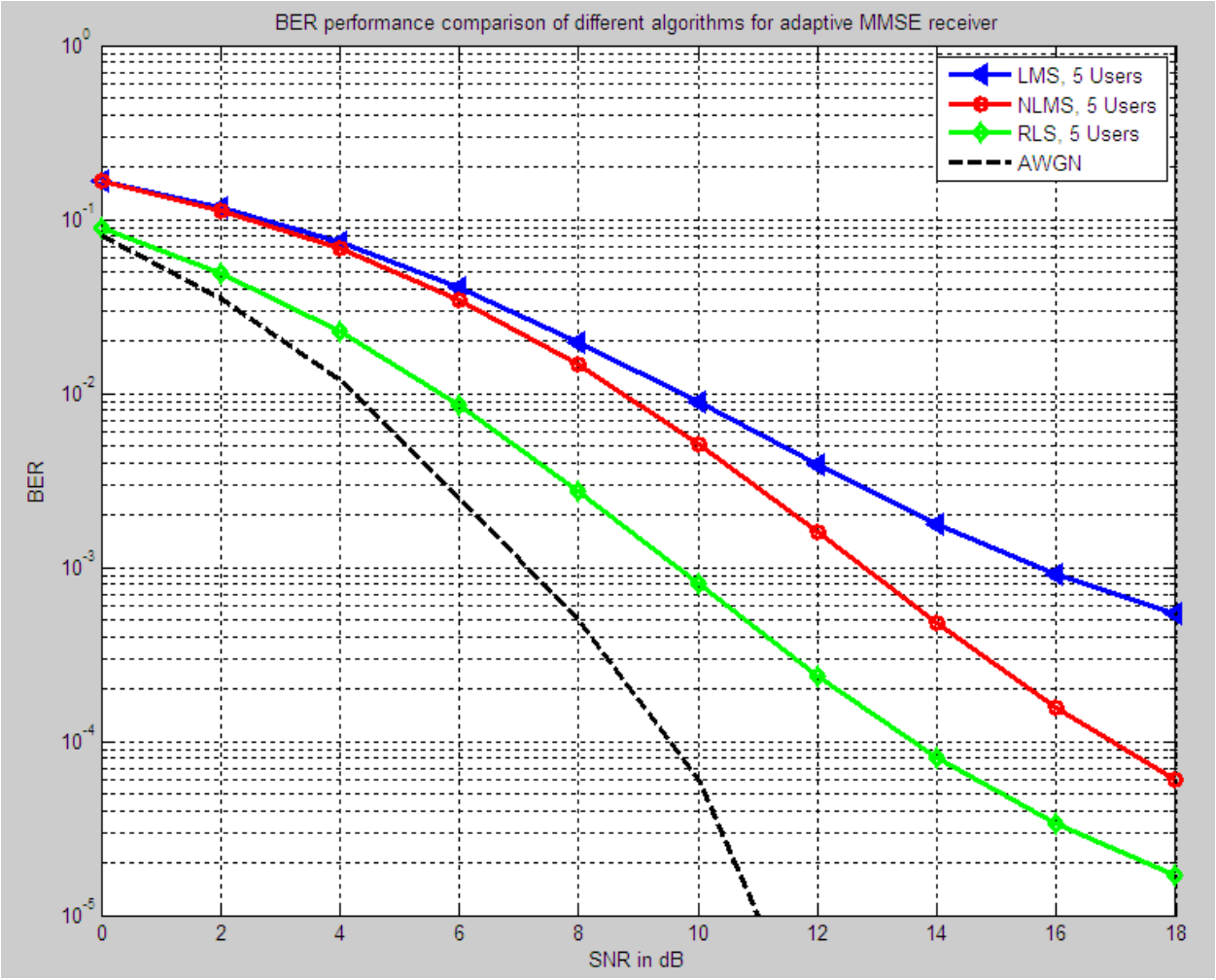

Figure 5.12: Performance comparison of different algorithms for adaptive MMSE receiver

5.4. Performance Comparison of RAKE and Adaptive MMSE Receivers

Figure 5.13 describes BER performance comparison of SRAKE and adaptive MMSE receivers for single user scenario. SRAKE receiver with 5 and 10 fingers is considered for comparison and the adaptive MMSE receiver uses three of the adaptive algorithms. In the simulation, DS-BPSK-UWB transmitted signal format is used and CM1 is considered. In addition, we use MRC technique for the SRAKE receiver.

From the given plot, we can see that adaptive MMSE receiver using all the three adaptive algorithms has by far better BER performance compared to SRAKE receiver with 5 and 10 fingers. For example, at BER of 0.01 adaptive MMSE receiver using RLS algorithm has a SNR gain of around 6dB compared to SRAKE receiver with 5 fingers.

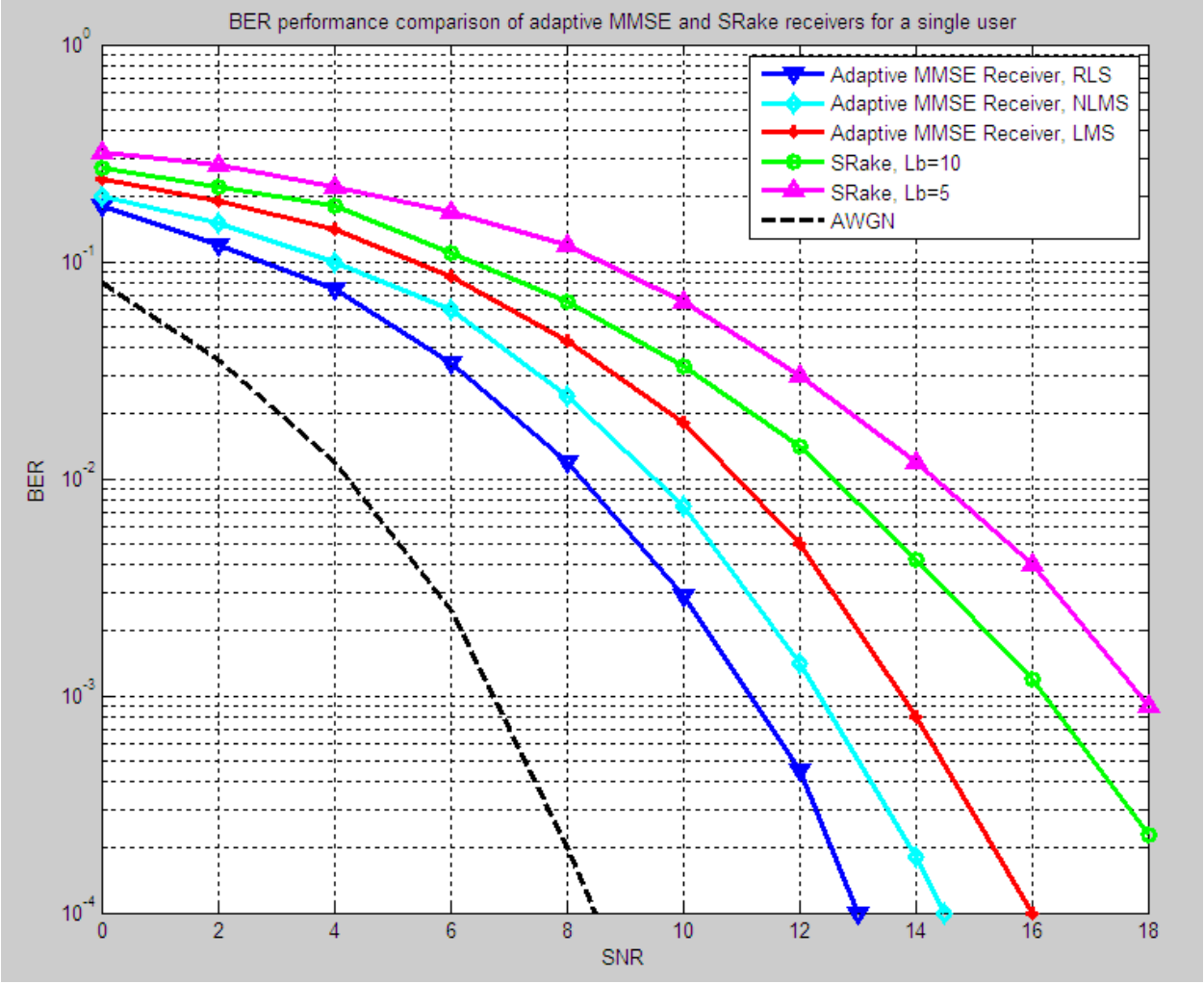

Figure 5.13: BER performance comparison of SRake and adaptive MMSE receivers

Chapter 6

Conclusion and Recommendations for Future Work

6.1. Conclusion

Ultra-wideband (UWB) communication is an emerging technology for wireless transmission in the 3.1-10.6 GHz unlicensed band with signal bandwidth of 500 MHz or greater. This technology is capable of transmitting more data in a given time than other existing technologies. Therefore, UWB technology can be used in various wireless personal area network (WPAN) applications. This technology has low complexity, low cost, and low power consumption. Single-band Impulse Radio (IR) is one of the approaches considered for UWB wireless communication systems. In this approach, the bit data is directly coded into base band short duration pulses. Those pulses have several properties, in particular a huge bandwidth (energy spread), high frequency components (carrierless transmission) and low power emissions (low interference with other coexisting wireless communication systems).

In this thesis, BER performance of RAKE and adaptive MMSE receivers is evaluated extensively considering different system parameters of the two receivers.

First, a detail BER performance analysis and comparison of RAKE receiver for different system parameters is presented. The parameters considered for BER performance analysis and comparison include RAKE combining techniques, RAKE receiver types, number of RAKE fingers, transmitted signal formats, channel types and bit repetition code lengths. The simulation results illustrate that an ideal ARAKE receiver using TH-BPSK-UWB transmitted signal format and MRC technique has the best performance. This performance can even be further improved by applying bit repetition coding at the transmitter. But since it is difficult to implement ARAKE receiver with large fingers practically, nearly the same performance can be attained using SRAKE receiver with medium number of fingers (5-15) and then applying MRC technique, TH-BPSK-UWB transmitted signal format and bit repetition coding at the transmitter. At SNR of 10dB (Figure 5.4), ARAKE receiver has a BER performance improvement of around 0.591, 0.201 and 0.181compared to PRAKE receiver with 5 fingers, PRAKE receiver with 10 fingers and SRAKE receiver with 5 fingers respectively. SRAKE receiver with 10 fingers and ARAKE receiver have nearly the same BER performance.

Then, an extensive BER performance analysis and comparison of adaptive MMSE receiver is provided for different number of user users using LMS, NLMS and RLS adaptive algorithms. The simulation results show that the BER performance of all the three algorithms falls rapidly as the number of interfering asynchronous users increase due to the effect of MUI. In addition, the results depict that adaptive MMSE receiver using RLS algorithm has the best performance compared to LMS and NLMS algorithms. At BER of 10^{-3} (Figure 5.12), adaptive MMSE receiver using RLS algorithm has a SNR gain of 3dB and 6.2dB compared to adaptive MMSE receiver using NLMS and LMS algorithms respectively.

Finally, BER performance comparison of SRAKE receiver with 5 and 10 fingers and adaptive MMSE receiver using LMS, NLMS and RLS algorithms is compared for single user scenario. The simulation result describes that adaptive MMSE receiver using all the three algorithms has by far the best performance compared to SRAKE receiver with 5 and 10 fingers. At SNR of 12dB (Figure 5.13), adaptive MMSE receiver using RLS algorithm has BER performance improvement of around 0.00105, 0.00455, 0.01455 and 0.02955 compared to adaptive MMSE receiver using NLMS and LMS algorithms and SRAKE receiver with 5 and 10 fingers respectively.

6.2. Recommendations for Future Work

The promising results of this thesis work led to expanding the thesis limits and widening the scope of the simulation to include the following possible approaches for future development. In this research, many important issues have not been dealt with, or have been considered with simplified assumptions. Hence, there are some areas in which the work of this thesis can be extended. Some topics for future research on RAKE and adaptive MMSE receivers for UWB wireless communication systems following the direction of this thesis include:

- *Performance analysis under practical power constraints:* In this thesis, perfect power control for each user is assumed which is not practically applicable. Thus, performance evaluations under conditions when user transmits at different power and received signals have different power level can be further investigated.
- *Impact of channel estimation and time synchronization:* In this thesis, simulations have been carried out assuming that the receiver has perfect channel knowledge and perfect time synchronization between the transmitter and receiver which deviates from the practical

situation. Thus, the impact of channel estimation and time synchronization errors on the system performance is another research area that needs further study.

- *Performance analysis for multiband scenario:* There two approaches for UWB wireless communication systems: *single-band* and *multi-band*. The single-band approach is implemented by direct modulation of information into a sequence of impulse like waveforms which occupy the available bandwidth of 7.5 GHz. The multi-band approach divides the available UWB bandwidth into smaller sub-bands, each with a bandwidth greater than 500 MHz. In this thesis, we only consider the single-band UWB wireless communication approach and this can be extended to multi-band approach.
- *Computational complexity and cost of implementation:* In this thesis, BER performance RAKE and adaptive MMSE receivers is evaluated for different system parameters without considering the computational complexity and cost of implementation of the receivers. Hence, analysis of computational complexity and cost of implementation of the two receivers could be another research area.

References

[1] X. Chen and S. Kiaei," Monocycle Shapes for Ultra Wideband System", *IEEE International Symposium on Circuits and Systems*, August 07, 2002.

[2] M. G. Khan, J. Nordberg, A.Mohammed, and I. Claesson, "Performance evaluation of RAKE receiver for UWB systems using measured channels in industrial environments," *Int. Conf. on Wireless Broadband and Ultra Wideband Systems*, March 2006.

[3] J. G. Proakis, *Digital Communications*, 4th ed., McGraw-Hill, New York, 2001.

[4] L. Jiabin and L. Zhonghua, "Adaptive MMSE receiver based DS-UWB indoor transmission scheme," *Wireless Communications, Networking and Mobile Computing, Int. Conference*, pp. 574-577, Sept. 2007

[5] I. Guvenc and H. Arslan, "On the Modulation Options for UWB Systems," *Proc. IEEE on* Military Communications Conference, vol. 2, pp. 892–897, Oct. 2003

[6] A. Rajeswaran, V.S. Somayazulu, J. R. Foerster, "RAKE performance for a pulse based UWB system in a realistic UWB indoor channel,"*Proc. IEEE International Conference on Communications*, vol.4, pp. 2879 - 2883, May 2003.

[7] Q. Li and L. A. Rusch, "Multiuser receivers for DS-CDMA UWB," *IEEE Conference on Ultra Wideband Systems and Technologies*, pp. 163-167, May 2002.

[8] G. Durisi, J. Romm, and S. Benedetto, "Performance of TH and DS UWB Multi-access Systems in Presence of Multipath Channel and Narrowband interference," *IWUWBS* 2003, Oulu, Finland, June 2003

[9] D. Cassioli, M. Z. Win, F. Vatalaro, and A. F. Molisch, "Performance of low-complexity Rake reception in a realistic UWB channel", *Proc. IEEE Int. Conf. on Communications*, pp. 763-767, May 2003

[10] J. R. Foerster et al, "Channel modeling sub-committee report final," IEEE P802.15-02/490r1 SG3a, IEEE P802.15-02/490r1-SG3a 1, Feb. 2003

[11] A. F. Molisch et al., "IEEE 802.15.4a channel model - final report," *Tech. Rep. Document IEEE* 802.15-04-0662-02-004a, 2005

[12] J. H. Reed, *An Introduction to Ultra Wideband Communication Systems*, Prentice Hall, 2005

[13] M. Z. Win and R. A. Scholtz, "Impulse radio: how it works," *IEEE Commun. Lett.*, vol. 2, no. 2, pp. 36–38, Feb. 1998.

[14] S. Haykin, *Adaptive Filter Theory*, 3rd Edition, Prentice Hall, New Jersey, 1996.

[15] A. A. M. Saleh and R. A. Valenzuela, "A statistical model for indoor multipath propagation," *IEEE J. Select. Areas Commun.*, vol. 5, no. 2, pp. 128–137, Feb. 1987.

[16] H. Sheng, A. M. Haimovich, A. F. Molisch, and J. Zhang, "Optimum Combining for Time Hopping Impulse Radio UWB Rake Receivers," *Proc. IEEE Conference on Ultra Wideband Systems and Technologies*, Reston, VA, November 2003.

[17] M. Pendergrass and W. C. Beeler, "Empirically based statistical ultra-wideband (UWB) channel model," Technical Report P802.15 02/240SG3a, Time Domain Corporation, Huntsville, AL, June 2002

[18] G. Durisi and S. Benedetto, "Performance Evaluation and Comparison of Different Modulation Schemes for UWB Multiaccess Systems," ICC 2003, Anchorage, Alaska, USA

[19] Federal Communications Commission, "Revision of Part 15 of the commission's rules regarding ultra-wideband transmission systems, first report and order," ET-Docket 98-153, FCC, Washington, DC, Feb. 2002.

[20] S. S. Ghassemzadeh et al., "A statistical path loss model for in-home UWB channels," *Proc. IEEE Conf. Ultra Wideband Syst. Technol.*, pp. 59–64, May 2002

[21] Paulo S.R. Diniz, *Adaptive Filtering: Algorithms and Practical Implementation*, 3rd Edition, Kluwer Academic Publishers, 2008.

[22] H. Sheng et al., "On the Spectral and Power Requirements for Ultra-Wideband Transmission," *IEEE International Conference on Communications*, Alaska, USA, May 2003.

[23] D. Cassioli, M. Z. Win, and A. F. Molisch, "The ultra-wide bandwidth indoor channel: from statistical model to simulations," *IEEE J. Select. Areas Commun.*, vol. 20, pp. 1247–1257, Aug. 2002.

[24] Bo Hu, Norman C. Beaulieu, "Accurate Evaluation of Multiple-Access Performance in TH-PPM and TH-BPSK UWB Systems," *IEEE Transactions on Communications*, Vol.52, No.10, October 2004.

[25] F. Zhu, Z. Wu, and C. R. Nassar, "Generalized fading channel model with applications to UWB," *Proc. IEEE Conf. Ultra Wideband Syst. Technol.*, pp. 13–17, 2002

[26] W.Siriwongpairat and K.J. Ray Liu, *Ultra-Wideband Communications Systems: Multiband OFDM Approach*, John Wiley & Sons, New Jersey, 2008

[27] R. J. Cramer, R. A. Scholtz, and M. Z. Win, "Evaluation of an ultra-wide-band propagation channel," *IEEE Trans. Antennas Propag.*, vol. 50, pp. 561–570, May 2002.

[28] Li Zhao, Alexander M. Haimovich, "Interference Suppression in Ultra-Wideband Communications," *Conference on Information Sciences and Systems*, the John Hopkins University, Mrach 2001

[29] M. L. Welborn, "System considerations for ultra-wideband wireless networks," *Proc. IEEE Radio Wireless Conf.*, pp. 5–8, Aug. 2001

[30] N. Boubaker and K. B. Letaief, "Ultra wideband DSSS for multiple access communications using antipodal signaling," *Proc. IEEE Int. Conf. Commun.*, vol. 3, pp. 11–15, May 2003

[31] J. Kunisch and J. Pamp, "Measurement results and modeling aspects for the UWB radio channels," *Proc. IEEE Conf. Ultra Wideband Syst. Technol.*, pp. 19–23, May 2002

[32] D.G. Brennan, "Linear diversity combining techniques", Proc. IRE, vol.47, no.1, pp.1075–1102, June 1959

[33] R. A. Scholtz, "Multiple access with time-hopping impulse modulation," *Proc. MILCOM Conf.*, Boston, MA, pp. 447–450, Oct. 1993

[34] D. G. Leeper, "Wireless data blaster," *Scientific American*, May 2002.

[35] H. Hashemi, "Impulse response modeling of indoor radio propagation channels," *IEEE J. Selected Areas Commun.*, vol. 11, no. 7, pp. 967–978, Sept. 1993

[36] S. Gezici, H. Kobayashi, H. V. Poor and A. F. Molisch, "Performance evaluation of impulse radio UWB systems with pulse-based polarity randomization in asynchronous multiuser

environments," *Proc. IEEE Conference on Ultra Wideband Systems and Technologies (UWBST 2004)*, Kyoto, Japan, May 18-21, 2004.

[37] H.V.Poor and S.Verdu, "Probability of error in MMSE multiuser detection," *IEEE Trans. Information Theory*, vol. 43, May 1997, pp.858-871.

[38] U. Madhow, "Blind adaptive interference suppression for direct-sequence CDMA," *Proc. IEEE*, vol. 86, pp. 2049–2069, Oct. 1998.

[39] J. R. Foerster, "The performance of a direct-sequence spread ultrawideband system in the presence of multipath, narrowband interference, and multiuser interference," *Proc. IEEE Conf. Ultra Wideband Syst. Technol.*, pp. 87–91, May 2002.

[40] R. J. Fontana, "Recent system applications of short-pulse ultra-wideband (UWB) technology," *IEEE Trans. Microwave Theory Tech.*, vol. 52, no. 9, pp. 2087–2104, Sept. 2004.

[41] H. Kikuchi. "UWB arrives in Japan," *Nikkei Electronics*, pages 95–122, February 2003.

[42] H. Fathallah and L. A. Rusch, "A subspace approach to adaptive narrowband interference suppression in DSSS," *IEEE Trans. Commun.*, vol. 45, pp. 1575–1585, Dec. 1997

[43] C. M. Canadeo, M. A. Temple, R. O. Baldwin, and R. A. Raines, "Code selection for enhancing UWB multiple access communication performance using TH-PPM and DS-BPSK modulations," *Proc. IEEE Wireless Commun. Network. Conf.*, pp. 678–682, Mar. 2003

[44] I. Oppermann et al., "UWB wireless sensor networks: UWEN—a practical example," *IEEE Commun. Mag.*, vol. 42, no. 12, pp. 27–32, Dec. 2004.

[45] V. S. Somayazulu, "Multiple access performance in UWB systems using time hopping vs direct sequence spreading," *Proc. IEEE Wireless Commun. Network. Conf.*, vol. 2, pp. 522–525, Mar. 2002

[46] S. Verdu, *Multiuser Detection*, Cambridge, U.K.: Cambridge Univ. Press, 1998.

[47] N. Boubaker and K. B. Letaief, "Ultra wideband DSSS for multiple access communications using antipodal signaling," *Proc. IEEE Int. Conf. Commun.*, vol. 3, pp. 11–15, May 2003

[48] T. Kaiser, Ed., *UWB Communications Systems: A Comprehensive Overview*, EURASIP Series on Signal Processing and Communications, Hindawi Publishing, New York, 2005.

[49] R. J. Fontana, ―Recent system applications of short-pulse ultra-wideband (UWB) technology," *IEEE Trans. Microwave Theory Tech.*, vol. 52, no. 9, pp. 2087–2104, Sept. 2004

[50] I. Bergel, E. Fishler, and H. Messer, ―Narrowband interference suppression in time-hopping impulse-radio systems," *Proc. IEEE Conf. Ultra Wideband Syst. Technol.*, pp. 303–307, 2002

[51] D. Porcino and W. Hirt, ―Ultra-wideband radio technology: potential and challenges ahead," *IEEE Commun. Mag.*, vol. 41, no. 7, pp. 66–74, July 2003.

[52] F. Ramirez-Mireles and R. A. Scholtz, ―Multiple-access performance limits with time hopping and pulse position modulation," *Proc. IEEE Military Commun Conf.*, pp. 529–533, Oct. 1998.

[53] M. Ghavami, L.B. Michael and R. Kohno, *Ultra Wideband Signals and Systems in Communication Engineering, Wiley & Sons*, 2nd Edition, 2004.

[54] R. A. Scholtz, ―Multiple access with time-hopping impulse modulation," *Proc. MILCOM Conf.*, Boston, MA, pp. 447–450, Oct. 1993.

[55] W. Malik, C. Stevens, and D. Edwards, ―Multipath effects in ultrawideband RAKE reception," *IEEE Trans. Antennas Propagat.*, vol. 56, no. 2, pp. 507–514, Feb. 2008.

[56] M.G. Di Benedetto, G. Giancola, *Understanding Ultra Wide Band Radio Fundamentals*, Prentice Hall Publications, USA, 2004.

[57] M. Tichy and J. Schier, "GSFAP Adaptive Filtering Using Log Arithmetic for Resource-Constrained Embedded Systems," *ACM Transactions on Embedded Computing Systems*, Vol. 9, No. 3, February 2010

[58] N. C. Beaulieu and B. Hu, ―A pulse design paradigm for ultra-wideband communication systems," *IEEE Trans. Wireless Commun.*, vol. 5, no. 6, pp. 1274-1278, June 2006.